MECHANOTRANSDUCTION OF SUBCELLULAR AMPK AND ITS ROLE IN BREAST CANCER CELL MIGRATION

A Thesis

Submitted to the Faculty

of

Purdue University

by

Hannah E. Steele

In Partial Fulfillment of the

Requirements for the Degree

of

Master of Science in Biomedical Engineering

May 2018

Purdue University

Indianapolis, Indiana

THE PURDUE UNIVERSITY GRADUATE SCHOOL
STATEMENT OF COMMITTEE APPROVAL

Dr. Sungsoo Na, Chair

Department of Biomedical Engineering

Dr. Hiroki Yokota

Department of Biomedical Engineering

Dr. Jong Eun Ryu

Department of Mechanical Engineering

Approved by:

Dr. Julie Ji

Head of the Graduate Program

ACKNOWLEDGMENTS

I would like to thank my mentor, Dr. Sungsoo Na, for his continual guidance and support. This study would not be possible without his careful direction, expertise, and encouragement. I am grateful for his time and effort to help me become a better researcher. I would also like to thank the members of my thesis advisory committee, Dr. Hiroki Yokota and Dr. Jong Eun Ryu for their support throughout my project.

I wish to thank the past and present members of the Na laboratory, Qiaoqiao Wan, Yunxia Guo, and ThucNhi TruongVo, for their training and help with research projects, as well as their encouragement and friendship.

Finally, I would like to thank my family and friends for their immeasurable love and support during my graduate studies.

TABLE OF CONTENTS

Page

LIST OF FIGURES

Figure Page

LIST OF ABBREVIATIONS

2D	Two-dimensional
3D	Three-dimensional
AIP	AMPK inhibitor peptide
AMPK	AMP-activated protein kinase
CAFs	Cancer-associated fibroblasts
CFP	Cyan fluorescent protein
ECM	Extracellular matrix
IFF	Interstitial fluid flow
ITP	Intra-tumoral pressure
FA	Focal adhesion
FAK	Focal adhesion kinase
FPs	Fluorescent proteins
FRET	Fluorescent resonance energy transfer
LKB1	Liver kinase B1
MMPs	Matrix metalloproteinases
SEM	Standard error of the mean
TGF-	Transforming growth factor beta
VEGF	Vascular endothelial growth factor
YFP	Yellow fluorescent protein

ABSTRACT

Steele, Hannah E. M.S., Purdue University, May 2018. Mechanotransduction of Subcellular AMPK and its Role in Breast Cancer Cell Migration. Major Professor: Sungsoo Na.

The biophysical microenvironment of the tumor site has significant impact on breast cancer progression and metastasis. The importance of altered mechanotransduction in cancerous tissue through the integrin-mediated signaling axis has been documented, yet its role in the regulation of cellular metabolism and the potential link between cellular energy and cell migration remain poorly understood.

In this study, we investigated the role of mechanotransduction (via Src and FAK) in AMP-activated protein kinase (AMPK) activation in breast cancer cells in response to interstitial fluid flow. Additionally, we explored the involvement of AMPK in breast cancer cell migration. An in-vitro three-dimensional (3D) cell culture model utilizing collagen-Matrigel matrices was used. Interstitial fluid flow was applied to the 3D cell-matrix construct inside a flow chamber. The sub-cellular signaling activity of Src, FAK, and AMPK was visualized in real-time using fluorescent resonance energy transfer (FRET). We observed that breast cancer cells (MDA-MB-231) are more sensitive to interstitial fluid flow than normal epithelial cells (MCF-10A) in the regulation of FAK and Src. AMPK was activated in the mitochondria of MDA-MB-231 cells by interstitial fluid flow, but not in other subcellular domains (i.e., cytosol, plasma membrane, and nucleus). Subcellular AMPK in MCF-10A cells did not respond to interstitial fluid flow. The inhibition of FAK or Src abolished flow-induced AMPK activation in the mitochondria of MDA-MB-231 cells. We also observed that global AMPK activation reduced MDA-MB-231 cell migration. Interestingly, specific

AMPK inhibition in the mitochondria reduced cell migration and blocked interstitial fluid flow-induced cell migration.

Our results suggest the linkage of FAK/Src and mitochondria-specific AMPK in mechanotransduction and the dual role of AMPK in breast cancer cell migration depending on its subcellular activation. Therefore, subcellular AMPK activation may play an important and distinct role in cancer invasion and progression.

1. INTRODUCTION

More than 80% of cancers in human adults are carcinomas cancers arising from the malignant transformation or mutation of epithelial cells [1], malignant cells form primary tumors that damage surrounding tissue and alter the biochemical and mechanical properties of the extracellular matrix (ECM). Changes in the mechanics of cancerous breast tissue include increased stiffness, interstitial fluid flow, and interstitial fluid pressure [2–9]. These physical changes increase the stresses experienced by breast cancer cells, encouraging a metastatic phenotype and migration away from the primary tumor site [3–5, 7–10]. Both cell sensing and migration responses are mediated by focal adhesions that connect the intracellular cytoskeletal network to the ECM. Focal adhesions transduce mechanical stimuli to cells via integrin-mediated signaling, which includes integrin-associated protein kinases Src and FAK. Both Src and FAK are up-regulated in cancer cells, enabling increased cell motility. One possible downstream target of Src and FAK is the master metabolic regulator AMPK. Global, cellular AMPK is down-regulated in cancer cells, but its paradoxical effects in tumor growth, proliferation, and migration suggest that AMPK may play antagonistic roles in various subcellular domains.

1.1 Epithelial breast tissue

1.1.1 Tissue and cell types

Breast tissue can be broken down into two major parts the mammary glands (and their connected ducts) and the supporting stroma. Mammary glands and ducts are composed of epithelial cells and make up 20% of total breast tissue [11]. Fig. 1.1 below shows the cross-sectional structure of a mammary duct. The duct is lined by three

types of epithelial cells luminal cells, myoepithelial cells, and epithelial progenitors [1]. It is from these ductal cells that most all breast cancers arise [1, 11, 12], and invasive luminal carcinoma is the most common type of breast cancer [13].

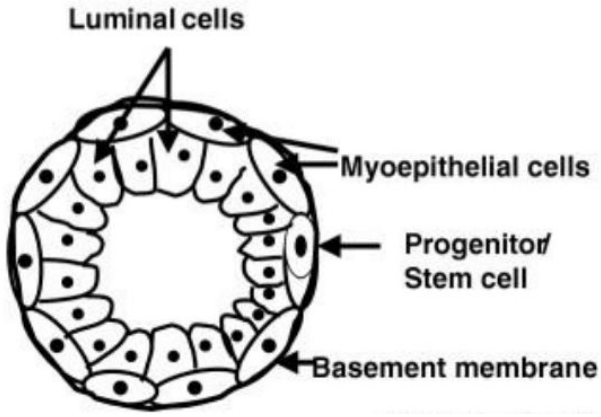

Fig. 1.1.: Diagram showing the luminal structure of a mammary duct [1].

The basement membrane around mammary ducts is composed of collagen IV, laminin, entactin, and proteoglycans [12, 13]. Surrounding the basement membrane of mammary ducts is the supporting stroma, which makes up 80% of breast tissue [11], interstitial dense connective tissue, loose connective tissue, and blood vessels. Major stromal cells include adipocytes, which remain in fat tissue, and fibroblasts that maintain and secrete/replace the ECM of connective tissue [3, 11].

1.1.2 Extracellular matrix

The extracellular matrix (ECM) is a dynamic amalgamation of water, proteins, and polysaccharides that surrounds and supports the cells within tissues [12]. The solid phase of ECM consists of collagen I, laminin, elastin, fibronectin, glycoproteins, and proteoglycans [11–13]. Glycoproteins are (glycosylated) proteins with saccharide/carbohydrate chains attached to their amino side-chains. Proteoglycans are heavily glycosylated proteins composed of a core protein with many glycosaminoglycan (GAG) side chains. Proteoglycans (i.e. heparin sulfate) form large complexes

with collagen fibers and act to stabilize and fill the ECM [12]. Collagen, elastin, and fibronectin form a fibrous mesh that fills and structuralizes the ECM of connective tissue. Type I collagen is the predominant fiber in ECM, and is therefore the primary regulator of tensile properties within the tissue [13]. Fibers support cells by providing adhesion sites for them to attach (focal adhesions). These cell-matrix adhesions enable intracellular tension homeostasis, migration, and mechanotransduction through the tissue [12]. Additionally, the liquid phase of ECM exerts fluid shear stress to embedded cells via interstitial fluid flow [7].

1.1.3 Interstitial fluid flow

Interstitial fluid, sometimes called tissue fluid, is the medium found within the ECM [7]. With every heartbeat, nutrient- and oxygen-rich plasma leaks from capillaries into the stromal space to nourish cells there. Most interstitial fluid returns to the cardiovascular system via post-capillary venules, and some filters through the interstitium toward the lymphatic vessels, creating regular interstitial fluid flow (IFF) [7]. The physiological IFF rate is estimated to range from 6-60 μm/s, creating a pulsatile shear stress of about 1 dyne/cm^2 (or 0.1 Pa) within the ECM [4]. The shear stress experienced by cells embedded in a porous ECM is likely higher around the cell surface, generating a shear stress of several Pascal on cells [6]. In healthy tissue, this shear stress is sensed and regulated by fibroblasts inside the ECM. Stromal fibroblasts exert tension on collagen fibers of the ECM via focal adhesions, contracting or relaxing to regulate fluid flow [2]. In cancerous tissue, however, IFF is highly irregular.

1.2 Epithelial breast cancer tissue

1.2.1 Tumor site ECM and IFF

Malignant, epithelial mammary cells form primary tumors out of mammary ducts and into the surrounding ECM. Tumor growth places unwanted pressure on its con-

fined ECM, increasing IFF [2,7]. Additionally, the internal tumor pressure (ITP) can be 100 times greater than surrounding healthy tissue, creating a pressure gradient outward from the tumor site [4,7]. This pressure gradient interrupts normal interstitial fluid flow patterns, which can no longer drain correctly, further increasing the rate of IFF and causing fluid build-up [7]. Rapidly proliferating tumor cells begin stimulating matrix metalloproteinases (MMPs) to break down collagen around the tumor. Cancer cells also secrete high levels of inflammatory cytokines that recruit immune cells to the site [12]. Additionally, increased IFF and tumor secretions prompt stromal fibroblasts to become cancer-associated fibroblasts (CAFs) [3]. CAFs begin depositing collagen I and III, laminin, elastin, and fibronectin at an unusual rate, increasing the fibrous density of the ECM even further [3,12]. In addition to fibrotic matrix deposition, CAFs secrete high levels of TGF- and VEGF, which enhance tumor growth and angiogenesis [3,4]. New (and irregular) blood vessels grow into the tumor to keep up with its metabolic expenditure [2,7]. Figure 1.2 (below) shows increased matrix deposition, immune cell response, and irregular blood vessel formation in tumorigenic tissue. The vicious cycle continues as increased ECM fibers, vessel density, and inflammatory cell recruitment contribute to increased interstitial fluid flow [2]. Abnormally high IFF in cancerous tissue and its consequences on the biophysical environment are known to promote cancer cell metastasis and invasion [3–5,7,9].

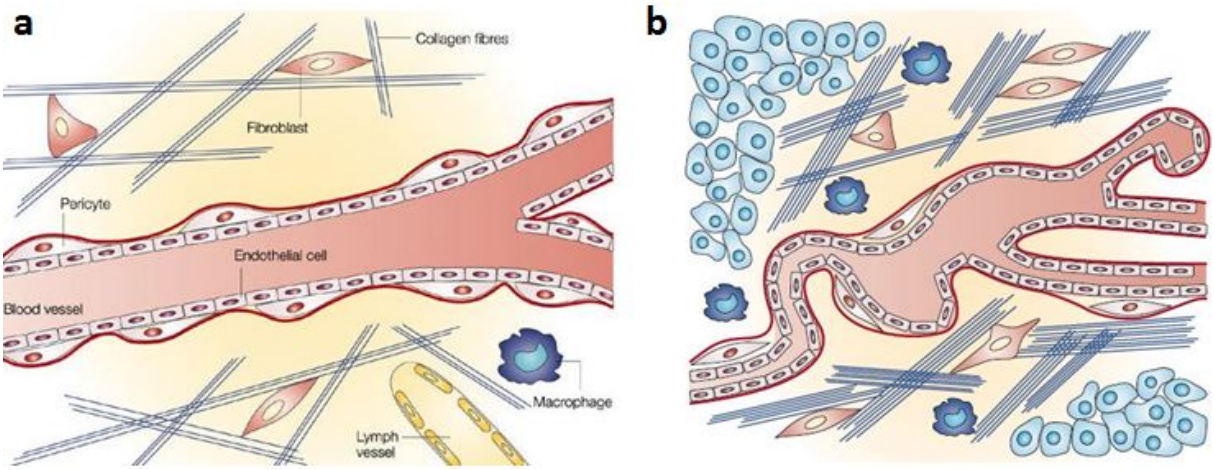

Fig. 1.2.: Illustration showing (a) normal connective tissue versus (b) cancerous tissue [2].

1.2.2 IFF in breast cancer migration

The tumor microenvironment is damaging to healthy mammary tissue, and may cause pain or discomfort to the patient. The real danger, however, is metastasis of breast cancer cells from the primary tumor site to distal parts of the body. The general steps of breast cancer metastasis are shown below in Figure 1.3. Once a primary tumor has been formed and vascularized, cells detach from the tumor site and migrate toward blood vessels [4, 10]. Individual cancer cells then squeeze through the endothelial lining of vessels and circulate through the blood stream to distal parts of the body. Finally, cells adhere to and exit the blood vessel, forming a secondary tumor site in adjacent tissue [10]. Breast cancer cells migrate preferentially to bone, where they degrade bone tissue and inhibit red and white blood cell production [14]. Ultimately, it is cancer cell metastasis, rather than primary tumor formation, that proves fatal. Since most patients are diagnosed after primary tumor formation and vascularization, the obvious target for cancer therapy is the prevention of metastasis. The interaction of both mechanical and biochemical stimuli and the complexity of intracellular signaling make the targets of initial metastasis difficult to identify.

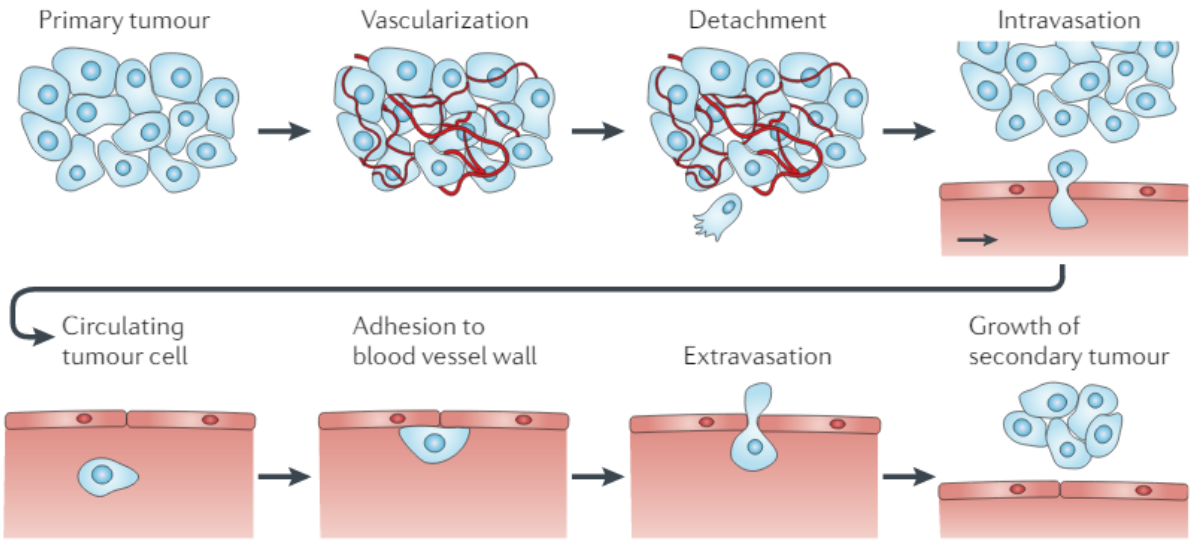

Fig. 1.3.: A schematic showing the metastatic cascade. Cancerous cells from the primary tumor are prompted to invade the ECM and migrate toward blood vessels. Cancer cells enter the bloodstream (intravasation), circulate to distal parts of the body, and exit the circulatory system (extravasation) to form a secondary tumor site [10].

As mentioned previously, increased IFF at the tumor site promotes cancer cell invasion. High IFF stimulates CAFs to deposit high volumes of ECM, namely collagen [3,12]. An ECM high in fibrous content increases breast cancer cell migration for two reasons. First, fibrotic deposition increases ECM stiffness, which is known to stimulate breast cancer cell migration in multiple cell lines, including highly metastatic MDA-MB-231 cells [4,7,8,10,12]. The stiffness of healthy mammary tissue has been estimated to be 200 Pa, while the stiffness of a breast cancer tumor can be as high as 4000 Pa [3]. The stiffness of the ECM around the tumor can be 100 times that of healthy tissue [7]. Second, a dense collagen matrix provides cancer cells with more adhesive surfaces to attach via integrin-mediated focal adhesions, which are necessary and active in migration [3,7,8,15]. High IFF can also stimulate focal adhesions directly via fluid shear stress. This integrin-mediated mechanotransduction has been repeatedly observed in vitro, where application of fluid shear stress promotes can-

cer cell migration [3–5, 7–9]. Finally, IFF induces cancer cell migration indirectly by prompting the secretion of cytokines and growth factors. In response to fluid flow, CAFs secrete high levels of TGF-β that encourage tumor growth, cancer cell survival, and a migratory phenotype [3, 16]. Irregular flow also stimulates the overproduction of growth factors such as FGF, EGF, or PDGF, all of which are known to stimulate cancer cell migration [3, 16, 17].

1.2.3 Epithelial-to-mesenchymal transition

The ability of cancer cells to migrate is largely determined by their phenotype. Regardless of whether invasion is stimulated by growth factors, cytokines, ECM stiffness, interstitial fluid flow, or a combination of these, a metastatic phenotype must be achieved. Individual cancer cell migration is initiated through a process called epithelial-to-mesenchymal transition (EMT) [Fig 1.4]. In this process, breast cancer cells lose their epithelial phenotype and transition to a mesenchymal/migratory phenotype [10, 16–18].

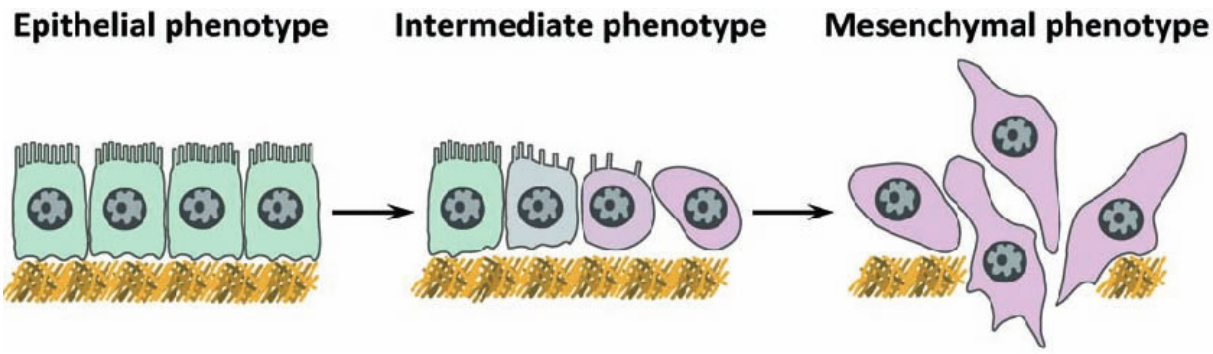

Fig. 1.4.: Schematic showing morphological shift of EMT [19].

Epithelial breast cells have distinct morphology tightly packed with strong adherens junctions between them [Fig. 1.5]. Adherens junctions are composed of transmembrane proteins called cadherins. E-cadherin (epithelial cadherin) is the primary cadherin in epithelial cell-cell binding.

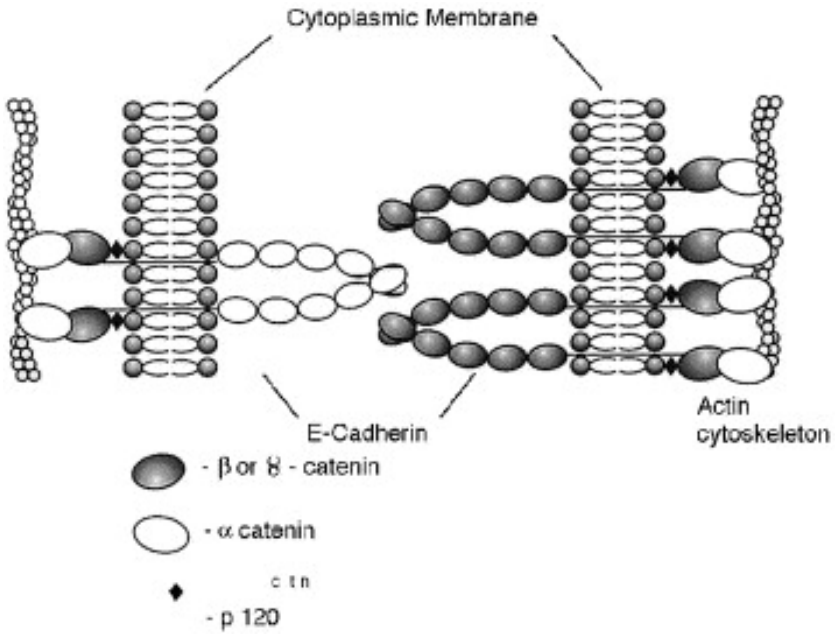

Fig. 1.5.: Diagram showing adherens junction between epithelial cells [18].

The extracellular domain of E-cadherin binds in a zipper fashion to the cadherins of adjacent cells. The cytoplasmic cadherin-catenin complex binds to the actin cytoskeleton within cells [18]. When a breast cancer cell undergoes EMT and becomes metastatic, there is a marked loss of E-cadherin expression [16–18, 20]. Loss of E-cadherin is followed by nuclear localization of β-catenin and subsequent up-regulation of EMT transcription factors like Snail and Twist [17]. EMT can be induced by TGF-β and various growth factors including EGF, PDGF, FGF, and VEGF [16, 17]. TGF-β activates the Smad pathway within epithelial cells, which ultimately act to up-regulate E-cadherin suppressors [16]. Once EMT is complete, cancer cells express high levels of vimentin [17] and focal adhesion kinase (FAK) [16], enabling cells to migrate individually. Cells with a mesenchymal phenotype are better able to resist apoptosis, adverse immune response, and chemotherapy [16]. Not all cancer cells migrate individually some carcinomas invade the surrounding tissue collectively [16]. In collective migration, one highly metastatic leader cell guides a linear array of cancerous followers while adherens junctions are maintained [16]. Some highly metastatic

breast cancer cell lines (such as MDA-MB-231 used in this study), however, only migrate individually and with a mesenchymal phenotype [21].

1.3 Cell signaling and mechanotransduction

Mechanical loading plays an important role in breast cancer metastasis. Changes in the mechanical properties of the ECM occur over weeks or months. Interstitial fluid flow, however, can induce cellular responses within seconds/minutes. Knowledge of upstream, integrin-mediated signaling is robust, and mechanical stimulation (via fluid flow) of integrins at focal adhesions initiates many signaling cascades. Namely, fluid flow-induced integrin activation plays a part in cancer cell migration. Here we discuss AMP-activated kinase (AMPK) as one potential downstream target of integrin-mediated mechanotransduction. Additionally, the role of subcellular AMPK in fluid flow-induced migration of breast cancer cells is considered.

1.3.1 Integrins, Src, and FAK

Integrins are transmembrane proteins consisting of heterodimeric and subunits. There are 16 types of α subunits and 8 β subunits which can form over 20 combinations, each corresponding to a different integrin. Integrins function as receptors for proteins of the ECM and connect them to the intracellular actin cytoskeleton. In both normal and cancerous epithelial breast cells, β1-integrins are most commonly expressed [22, 23]. β1-integrins bind to type I and type IV collagen, fibronectin, vitronectin, or laminin, depending on their α subunit. The extracellular domain of β1-integrins acts as the receptor and binding site for components of the ECM. Integrin-matrix binding induces integrin clustering at the plasma membrane and the formation of actin stress fibers within cells [22, 24]. The cellular tension within actin filaments is regulated by Rho GTPases (RhoA, Rac1, and Cdc42) to maintain structural homeostasis within the ECM and to mediate contractile forces in cell migration [24]. Contacts between integrin clusters and the ECM are termed focal adhesions

and are sites of mechanical force transmission/signaling. In this way, integrins act as the major mechanosensors for cells. The cytoplasmic domain of β1-integrin interacts with intracellular signaling molecules or adaptor proteins that connect it to the actin cytoskeleton [8, 22, 24]. These proteins include talin, paxillin, tensin, vinculin, FAK and Src [8, 9, 12, 24].

Fluid flow-induced shear stress exerted on metastatic breast cancer cells results in β1-integrin activation [5, 7–9, 12]. Signals initiated at these focal adhesions are then transduced into cells via activation of integrin-associated tyrosine kinases namely, Src and FAK [8, 9, 12, 22, 24]. During the formation of focal adhesions, FAK is recruited to sites of integrin clustering. It is unclear whether FAK associates directly with the β1 subunit of integrin or depends on the co-localization of adaptor proteins talin and paxillin [22]. Nonetheless, FAK is the first tyrosine kinase associated with the cytoplasmic tail of integrin. Upon integrin activation, FAK auto-phosphorylates at its Tyr-397 residue which creates a high-affinity Src binding domain (SH2) [22]. Src then binds to FAK, altering its regulatory tyrosine residue and creating a Src-FAK complex that can phosphorylate other molecules near the focal adhesion [22]. One known downstream target of Src and FAK is the family of Rho GTPases, which is activated by Src/FAK to increase cell motility [24].

FAK and Src are both highly expressed in metastatic breast cancer cells [24–26]. FAK is necessary for cell adhesion and migration; therefore, inhibition of FAK disassembles focal adhesions, stunts tumor growth/progression, and blocks cancer cell migration [8,24,25]. Similarly, selective inhibition of Src hinders cancer cell migration and ECM attachment [26]. It makes sense that inhibition of focal adhesion proteins would discourage cell migration, since the motility of cells depends on their ability to pull on the ECM. Just as β1-integrin activation can be initiated by flow-induced shear stress, Src and FAK can also be activated by IFF. Additionally, integrin-Src-FAK signaling due to interstitial fluid flow is connected to increased migration of breast cancer cells [5, 7–9, 12]. MDA-MB-231 cells embedded in 3D collagen gel showed

augmented migration in response to applied fluid flow, but inhibition of Src or FAK decreased their migratory response [5].

1.3.2 AMPK

Another potential downstream target of Src/FAK is the metabolic regulator AMPK. AMP-activated kinase (or AMPK) is a heterotrimeric kinase that senses and regulates cellular energy [27–30]. AMPK is composed of three subunits one catalytic α subunit and two regulatory subunits (β and γ). The γ subunit has four sequence repeats that function as four adenine nucleotide-binding domains. One domain is always bound to AMP, one is always free, and two are competitively bound by AMP, ADP, or ATP [29]. In this way, AMPK is able to sense the ratio of AMP and ADP to ATP, which is the usable form of energy in the cell. As the ratio of AMP:ATP increases, the amount of viable energy inside the cell drops, and AMPK is activated. On a molecular level, AMPK is activated when AMP binds to one of the competitive binding domains of the γ subunit [29]. AMPK can also be activated via phosphorylation of its α subunit by the well-known tumor suppressor LKB1 [29, 30]. The effects of AMPK activation include decreased cell growth and differentiation, increased ATP conservation/production, and inhibited anabolic processes [30]. In a broad sense, AMPK is activated as a result of metabolic stress, which is often a product of mechanical stress on the cell. Since mechanical stress is often transmitted through the cell via integrin-mediated signaling, AMPK may be a downstream target of Src/FAK activation.

1.3.3 Role of AMPK in cancer

As mentioned previously, AMPK is a direct substrate of tumor suppressor LKB1; however, in cancerous cells, LKB1 is mutated while AMPK is not [30]. Regardless, AMPK has also been considered a metabolic tumor suppressor since it regulates the growth and proliferation of cells. AMPK activity is always diminished in breast

cancer, and activating AMPK in metastatic cancer cells inhibits growth [27,28,30,31]. Augmented AMPK activity is known to attenuate cancer cell migration [27, 28, 31], and AMPK is believed to help regulate cell motility by controlling microtubule dynamics [31]. The efficacy of clinical AMPK activators in preventing tumor progression and metastasis is attributed in part to the inhibition of cell migration [31]. In spite of AMPK down-regulation in tumor cells, AMPK has garnered much attention for having dual functions in cancer. For example, when AMPK is on it stimulates mitophagy and enhances the metabolic flexibility/survival of cancer cells; however, AMPK activation also stunts tumor growth and proliferation [29, 30]. When AMPK is off it enables unchecked cancer growth and proliferation, but the metabolic plasticity of cells is diminished [29, 30]. The paradoxical nature of AMPK in cancer has led many to believe that the role of AMPK may vary based on its subcellular location [30, 32]. For example, ovarian cancer cells in 3D collagen gel display co-localization of AMPK activation with mitochondria at the leading edge of cells during migration [33]. If global AMPK activation reduces cancer cell migration [27, 31], but organelle-specific AMPK activity increases during migration, how might subcellular AMPK activation in cancer cells vary under mechanical stress?

1.4 FRET-based biosensors

FRET (fluorescent resonance energy transfer) microscopy was used to monitor kinase activity in various subcellular domains during interstitial fluid flow experiments. FRET-based biosensors are accurate tools for visualizing molecular activity inside living cells with high spatiotemporal resolution [34, 35]. FRET-based biosensors can be manufactured by fusing donor and acceptor fluorescent proteins to additional binding domains capable of conformational change [34, 35]. For example, consider the protein kinase FAK. A FRET-based biosensor for cytosolic-FAK contains a cyan fluorescent protein (CFP) donor, an SH2 binding domain, a FAK substrate peptide, and a yellow fluorescent protein (YFP) acceptor [Fig. 1.6]. In an inactive state, the fluorescent

proteins are in close proximity, which allows FRET from the CFP to the YFP. Cyan excitation (433 nm) of the biosensor gives yellow emission (527 nm) [36]. When cytosolic-FAK is activated, it will phosphorylate the FAK substrate of the biosensor. Upon phosphorylation of the substrate, it will bind to the SH2 domain. This causes a conformational change, separating the fluorescent proteins. Separation eliminates the FRET from CFP to YFP. In an active conformation, the biosensor will emit high CFP and low YFP signals. Therefore, the activation of FAK can be monitored over time using the ratio CFP/YFP [36]. The same is true for visualizing Src kinase activity [37, 38].

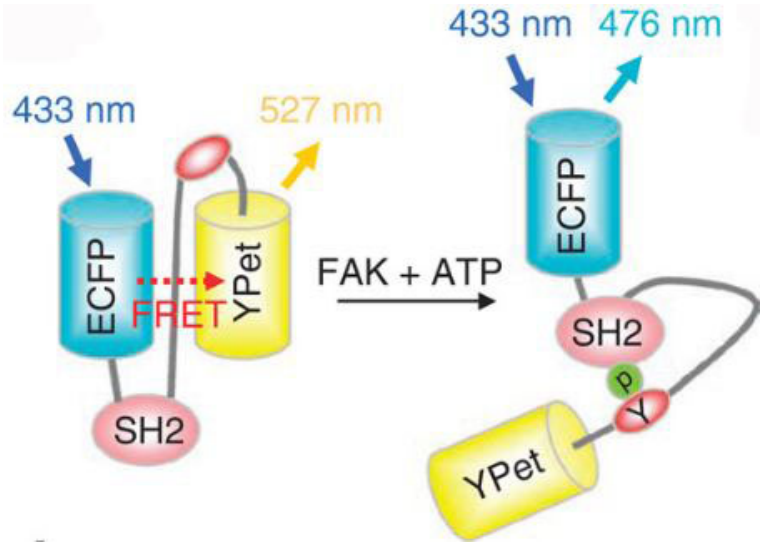

Fig. 1.6.: Structure and function of a FRET-based FAK biosensor [36].

FRET biosensors can also be specified to target subcellular domains. For example, Lyn-Src and Lyn-FAK biosensors were designed to observe Src and FAK activity at lipid raft regions of the plasma membrane. These membrane-specific biosensors were constructed by attaching palmitoylation sites at the N-termini of the biosensors, which ensure the biosensors are membrane-bound [38].

FRET biosensors for AMPK operate on the same general mechanism [Fig 1.7a]. AMPK biosensors contain a CFP, an FHA1 binding domain, an AMPK substrate

peptide, and a YFP variant (cpVE172) [32]. The difference is that an inactive conformation is characterized by separated fluorescent proteins, rather than proximal ones. Once AMPK phosphorylates the AMPK substrate peptide, it binds to the FHA1 domain. This brings the fluorescent proteins together, enabling FRET from CFP to YFP. Thus, AMPK activation can be observed via changes in the emission ratio YFP/CFP [32]. AMPK biosensors can also be designed to target specific subcellular locations [Fig.1.7b]. Different fusion sequences enable attachment to the following organelles: nucleus (Nuc-AMPK), plasma membrane (PM-AMPK), and mitochondria (Mito-AMPK) [32]. The ability to observe protein activation on a subcellular level makes FRET biosensors valuable tools for live cell imaging.

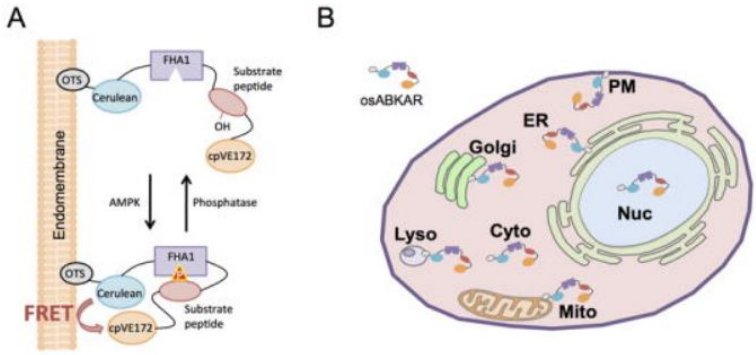

Fig. 1.7.: Schematics showing (A) the simplified structure of a membrane-bound AMPK FRET biosensor and (B) the locations of subcellular AMPK biosensors [32].

2. METHODS

2.1 Biosensors and plasmids

FRET biosensors were used to observe subcellular activities of Src, FAK, and AMPK in real time. The development and specificity of these biosensors were previously described [32, 36, 37]. The Src biosensor contains a cyan fluorescent protein (CFP) and the SH2 domain from c-Src, connected by a flexible linker to a yellow fluorescent protein (YFP) and Src substrate peptide [37]. Similarly, the FAK biosensor is comprised of a CFP, SH2 domain, YFP, and FAK substrate peptide [36]. Both Src and FAK biosensors (Lyn-Src and Lyn-FAK, respectively) were designed to target the lipid raft of the plasma membrane. Lipid raft-targeting biosensors were used for these tyrosine kinases because that is where mechanosensitive integrins reside. The AMPK biosensors consist of a CFP, an FHA1 binding domain, an AMPK substrate peptide, and a YFP variant (cpVE172). Subcellular AMPK FRET plasmids included Cyto-AMPK, PM-AMPK, Nuc-AMPK, and Mito-AMPK. An AMPK inhibitor peptide (Tom20-mChF-AIP) was used to specifically inhibit Mito-AMPK. The development and accuracy of Tom20-mChF-AIP was previously described [32]. Tom20-mChF -AIP acted as a preferential substrate to be phosphorylated by Mito-AMPK.

2.2 Chemical reagents

PP2 (Sigma, 10 μM) was used to inhibit Src activity, and PF573228 (Sigma, 1 μM) was used to inhibit FAK. Compound C (Millipore Sigma, 5 μM) was used as a global AMPK inhibitor. Previous studies also used a working concentration of 5 μM for the MDA-MB-231 breast cancer cell line [39, 40]. A769662 (Tocris, 25 μM) was used as a global AMPK activator.

2.3 Cell culture and transfection

The human breast cancer cell line MDA-MB-231 was used. MDA-MB-231 cells are triple negative, meaning they do not express estrogen or progesterone receptors and do not have amplified HER-2/neu. MDA-MB-231 cells were cultured in Dulbeccos modified Eagles medium (DMEM, Lonza) supplemented with 10% FBS (Gibco) and 1% penicillin/streptomycin (Lonza). The MCF10A human mammary epithelial cell line was also used to represent normal non-tumor breast cells. MCF10A cells were cultured in DMEM/F12 (Gibco) supplemented with 10% FBS (Gibco), 1% penicillin/streptomycin (Lonza), 200 ng/mL human recombinant EGF, 50 μg/mL hydrocortisone, and 20 μg/mL insulin (Sigma). All cells were maintained at 37 °C and 5% CO_2 in a humidified incubator. Lipofectamine LTX (Invitrogen) was used to transfect biosensors/plasmids into both cell types. During transfection, cells were incubated in OPTI-MEM (Gibco) serum-free, antibiotic-free media for at least 4 hours. Low serum (1% FBS), antibiotic-free DMEM (Lonza) was then added, and cells were incubated overnight. Cells were transfected 20-28 hours before imaging experiments. Prior to experimentation, transfected cells were transferred to type I collagen-coated glass-bottom dishes or μ-slide cell culture chambers (Ibidi) and incubated for at least 2 hours.

2.4 Collagen-Matrigel preparation

For 3D experiments, cells were seeded in type I collagen-Matrigel. As mentioned previously, the ECM of mammary tumors is primarily composed of type I collagen with small amounts of type IV collagen and laminin from the basal lamina of mammary ducts [12,13]. For this reason, a small amount of basal-lamina derived Matrigel was added to type I collagen for 3D culture. Collagen gel was prepared by adding 1 part chilled, antibiotic-free DMEM (10X) to 8 parts PureCol type I collagen solution (Advanced BioMatrix, 3 mg/mL). Next, 1 part Matrigel (Corning, 9.8 mg/mL) was added to the DMEM/collagen solution. The final concentration of type I collagen was

2.4 mg/mL. The pH of the mixture was adjusted to 7.4 using sterile NaOH or HCl. The complete collagen-Matrigel solution was warmed to room temperature, and cells were suspended in the mixture at a density of 1x10^6 cells/mL. For 3D experiments that did not require fluid flow, 100 μL of the solution (containing cells) was pipetted into a glass-bottom dish. For 3D interstitial fluid flow experiments, 100 μL of the mixture was injected into a 0.6 μ-slide cell culture chamber (Ibidi). Cell-gel samples were incubated for 2 hours at 37 °C and 5% CO_2 to form gel. Once gelation was complete, low-serum (1% FBS), antibiotic-free DMEM was added to each dish/chamber, and the samples were incubated for at least 1 hour before imaging.

2.5 Shear stress application

Fluid-flow induced shear stress was applied to both 2D and 3D cell samples grown in μ-slide cell culture chambers (Ibidi). For 2D samples, unidirectional flow was applied using a peristaltic pump (Cole-Parmer). The shear stress applied in 2D, which was 10 dyne/cm^2, was regulated by controlling the flow rate of the pump. The necessary flow rate was calculated using the following equation [41]:

$$\tau = 136.1\ \eta\ \phi$$

In this equation, τ represents shear stress, η is viscosity of the flow media (DMEM, 0.0072 dyne s/cm^2), and ϕ is the volumetric flow rate. To achieve a shear stress of 10 dyne/cm^2 in the flow chamber, a flow rate of 10.6 mL/min was employed. Before each experiment, the 2D flow chamber and sterile connective tubing was filled with phenol red-free DMEM (HyClone) supplemented with 1% FBS and maintained at 37 °C [Fig. 2.1a].

For 3D collagen gel samples, unidirectional, pulsatile (0.2 Hz) flow was applied using a syringe pump (Harvard Apparatus, PHD ULTRA). Three different flow rates (2, 5, 10 μL/min) were used to generate a range of shear stresses on the suspended cells. The flow chamber was connected to the syringe pump via sterile tubing filled

with FluoroBrite DMEM (Gibco) with 1% FBS. A 13mm filter was placed at the outlet of the flow chamber [Fig. 2.1b].

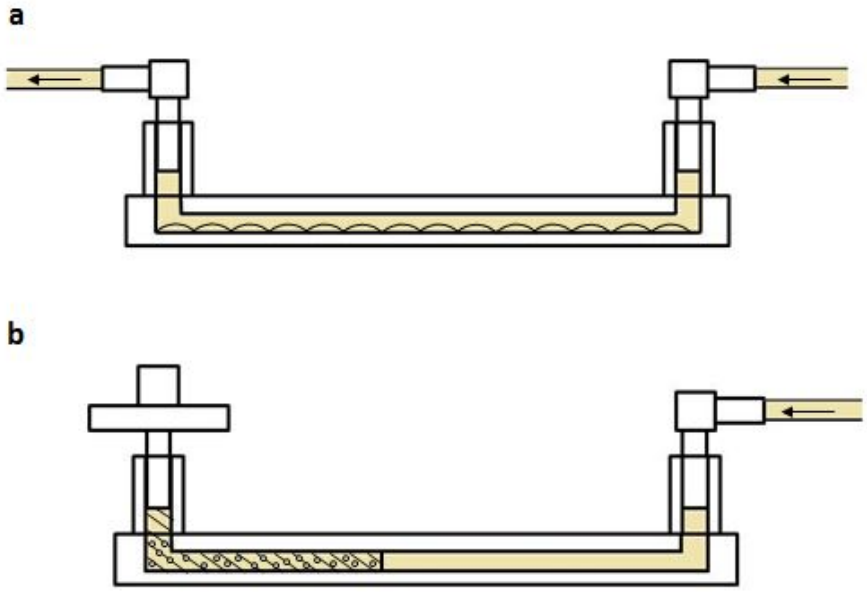

Fig. 2.1.: Diagrams showing the experimental setup for (a) 2D and (b) 3D flow chambers.

2.6 Collagen-Matrigel characterization and compaction

The interstitial flow speed through the collagen gel was calculated by measuring the intensity of fluorescent molecules moving through the porous cell-gel construct over time. First, fluorescent images were taken of collagen gel inside the flow chamber (before the addition of fluorescent probes), providing a reference for background intensity. Next, Alexa Fluor 594-conjugated bovine serum albumin (BSA-594, Thermo Fisher, 50 μg/ml) was added to the FluoroBrite DMEM (Gibco) that perfused the flow chamber. Using the syringe pump, the fluorescent media was pushed through the gel construct at known volumetric flow rates (2, 5, 10 μL/min) [Fig 2.2a]. Fluorescent images were obtained every minute for 10 minutes to track the perfusion of BSA-594 through the collagen gel. After each experiment, maximum intensity images were

captured from regions completely saturated by BSA-594. Interstitial flow speed was calculated from the following equation [42]:

$$v = \frac{L(I_2 - I_1)}{(I_{max} - I_b)(t_2 - t_1)}$$

L represents the length of the image (gel region being measured), and I_2 and I_1 are the fluorescent intensity values taken at time t_2 and t_1, respectively. I_{max} is the maximum fluorescent intensity, and I_b is the minimum/background intensity. The interstitial flow speed for each volumetric flow rate is shown below in Fig. 2.2b.

This range of interstitial flow speed yields a corresponding range of fluid shear stress exerted on cells embedded in our collagen-Matrigel. Due to the small cross-sectional area of the flow chambers and the porous nature of the gel, values for fluid shear stress are difficult to calculate. Any approximation of shear stress would be prone to error; however, we did estimate the permeability of our gel. Methods to determine the Darcy permeability (k) of type I collagen gel (2.5 mg/mL), containing cells at a density of $1*10^6$ cells/mL, have been characterized previously [43]. The Darcy permeability in Wang and Tarbells study was found to be $9*10^{-9}$ cm^2. Our gel, however, consisted of not only type I collagen (2.4 mg/mL), but also a small amount of Matrigel (Corning, 0.98 mg/mL). The primary components of Matrigel, which make up 98% of the mixture, are fibrous laminin and type IV collagen [44]. These added components should increase the density of the fibrous mesh within collagen gel, therefore decreasing Darcy permeability. This means the upper limit of Darcy permeability for our gel is close to $9*10^{-9}$ cm^2. On the other side of the spectrum, a polymerized gel formed from Matrigel alone (12 mg/mL) yields a Darcy permeability around $2.44*10^{10}$ cm^2 [45]. This value represents the lower limit of permeability for our collagen gel since the total concentration of fibrous molecules (collagen and laminin) in our gel is 3.4 mg/mL, nearly one quarter the concentration of Matrigel alone. Therefore, the Darcy permeability of our collagen-Matrigel lies in the range of $2.44*10^{10}$ to $9*10^{-9}$ cm^2.

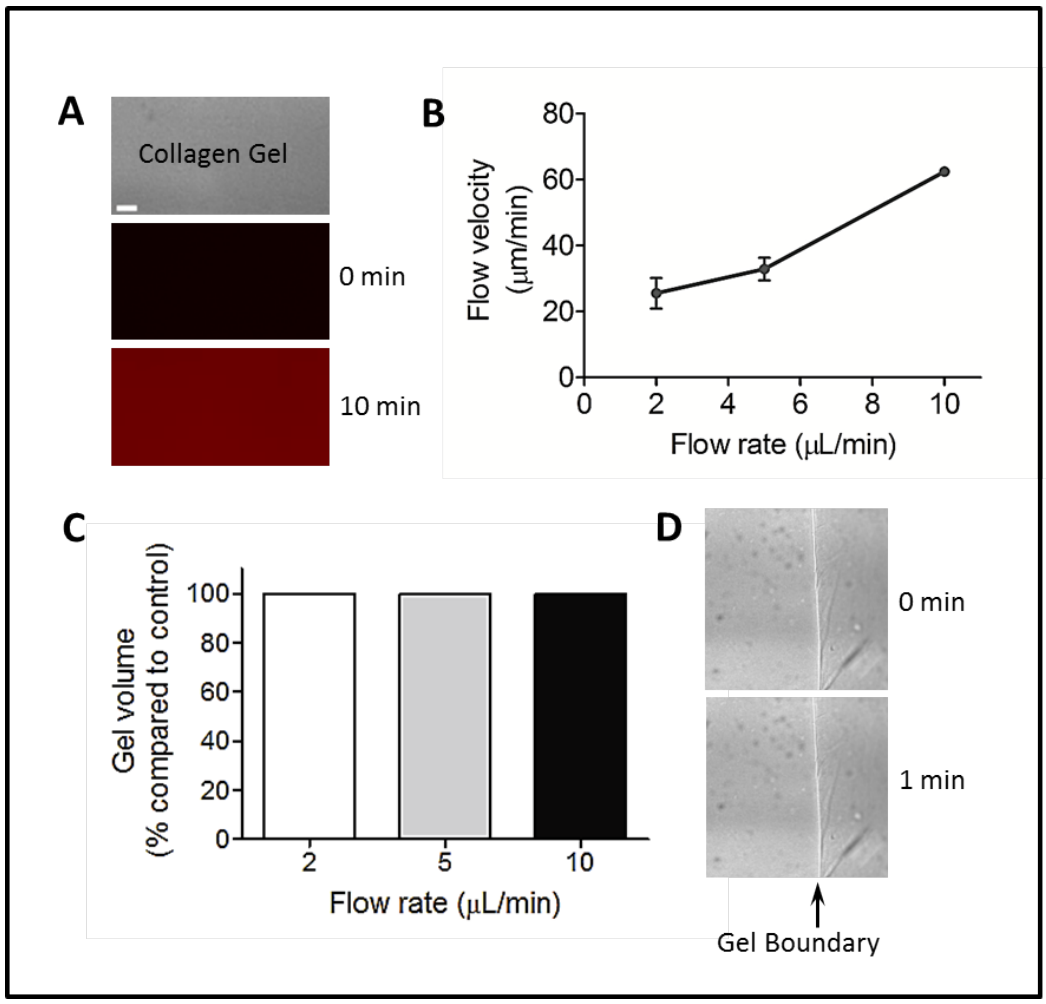

Fig. 2.2.: (A) Fluorescent intensity of BSA-594 before (0 min) and after 10 minutes of constant volumetric flow through collagen-Matrigel in a flow chamber. Scale bar, 10 μm. (B) Flow velocity (μm/min) of media through a collagen-Matrigel construct under various volumetric flow rates (μL/min), n=4. (C) Percent gel volume compared to control (100%) showing the compaction of collagen-Matrigel scaffolds under various volumetric flow rates, n=4. (D) DIC images showing negligible compaction of gel construct after 1 minute of fluid flow (10 μL/min).

The collagen gel (2.4 mg/mL) used was quite soft (with a stiffness on the order of 10^2 Pa), and a volumetric flow rate of 20 μL/min often ripped or pulled the collagen construct from the wall of the flow chamber. For this reason, compaction experiments were performed to ensure that interstitial fluid flow was not compressing suspended cells under 2, 5, or 10 μL/min volumetric flow rates. DIC images were captured

every 10 seconds for 1 minute to monitor initial deformation under unidirectional flow. Volumetric change of the cell-gel construct was calculated by measuring the movement of the gel edge in the direction of flow. Compaction experiments were repeated four times for each flow rate. Results showed virtually no compaction of the collagen gel under interstitial fluid flow [Fig. 2.2c].

2.7 Random migration assay

A random migration study was conducted to investigate the role of AMPK in cancer cell migration. All migration experiments were completed in 2D inside μ-slide flow chambers coated with type I collagen (PureCol, 100 μg/mL). MDA-MB-231 cells were first incubated for 30 minutes with CellTracker Green CMFDA fluorescent dye (Thermo Fisher, 20 μM). For migration under flow, cells were then seeded at low (10-20%) confluency on μ-slide flow chambers and incubated for 2 hours, giving them just enough time to attach. Flow chambers were then subjected to 2D fluid flow (10 dyne/cm^2) for 8 hours. For migration assays without flow, fluorescent cancer cells were seeded at low confluency inside flow chambers and incubated for 1.5 hours. After healthy cell attachment, floating cells were removed by replacing the media, and some samples were treated with Compound C (5 μM) or A769662 (25 μM). The treated cells were then incubated another 30 minutes before imaging. Antibiotic-free, phenol red-free DMEM (1% FBS) was used for all migration experiments. Flow chambers were kept at 37 °C and 5% CO_2 inside a humidified incubation chamber (Ibidi) during the migration assay. Fluorescent (GFP) and DIC images were captured every 5 minutes for 8 hours. Imaging regions were selected to include multiple isolated cells, away from the chamber walls and free to migrate randomly [46].

2.8 Microscopy and image analysis

All images were captured using a Nikon Ti-E inverted microscope equipped with an EMCCD camera (Photometrics, Evolve 512) and Perfect Focus System (Nikon).

FRET images were acquired using CFP 438 excitation, CFP 483 emission, and YFP 542 emission wavelength (nm) filters. Green fluorescent images were captured using a GFP 522.5 emission wavelength (nm) filter. To reduce photo-bleaching, a neutral density (ND) 32 filter was used to control the HG lamp (Nikon). For 3D interstitial fluid flow experiments, FRET and DIC images were taken every 2 minutes for 1 hour using a 40x objective. FRET ratio images for Src, FAK, and AMPK biosensors were created using NIS-Elements software (Nikon) and ImageJ. Representative Src and FAK cell images were generated as the emission ratio of CFP/YFP. In contrast, AMPK cell images were generated as the FRET emission ratio of YFP/CFP. For migration experiments, time-lapse images (DIC and GFP) were taken every 5 minutes for 8 hours using a 15x objective. Cell tracking was conducted using the ImageJ plugin TrackMate (Fiji) [47]. Cells used for tracking were chosen based on several parameters. Free/isolated cells that stayed within the image frame, did not divide, and did not die during the 8 hours were selected. Average distance traveled and average migration speed was calculated in Excel (Microsoft).

2.9 Statistical analysis

All statistical data are shown as the mean ± standard error of the mean (SEM). Statistical significance between multiple groups was determined using one-way analysis of variance (ANOVA) with Dunnetts post hoc test. Statistical significance between two groups was assessed using Students t-test. All statistical analysis was completed using Prism 5 software (GraphPad). A p-value less than 0.05 was considered statistically significant (*).

3. RESULTS

3.1 Interstitial fluid flow regulates Lyn-Src and Lyn-FAK in a flow magnitude-dependent manner

Fluid flow-induced shear stress initiates signals at focal adhesions that are transduced into cells by tyrosine kinases Src and FAK [5,7–9,12,22,24]. We investigated the shear mechanosensitivity of membrane-bound Src and FAK in both metastatic breast cancer (MDA-MB-231) and non-tumor epithelial breast (MCF-10A) cells grown in 3D culture. Cells were transfected with either Lyn-Src or Lyn-FAK and suspended in 3D collagen-Matrigel. Cell-gel mixtures were injected into separate flow chambers, and mechanical load was applied via interstitial fluid flow. Cells were subjected to no flow for 6 minutes, and then to 2, 5, or 10 μL/min fluid flow rates for 1 hour [Fig. 3.1.]. Lyn-Src and Lyn-FAK activity was measured by observing changes in CFP/YFP emission ratios. Application of 10 μL/min fluid flow induced activation of Lyn-FAK in cancer cells (49.9% increase at 60 min) but not in normal cells. Application of lower flow rates (2 or 5 μL/min) did not alter Lyn-FAK activity in either cell type. Lyn-Src was regulated in a flow magnitude-dependent manner in MDA-MB-231 cells. The 5 and 10 μL/min flow rates activated Lyn-Src (46.8% and 49.6% increase, respectively, at 60 min) with similar efficacy. The lowest flow rate of 2 μL/min activated Lyn-Src (14.1% increase at 60 min) to a lesser degree. Lyn-Src activation was less sensitive to interstitial fluid flow in MCF-10A cells. High fluid flow (10 μL/min) increased Lyn-Src activity by 12.8% at 60 minutes. Interestingly, an intermediate flow rate of 5 μL/min decreased Lyn-Src activity by 7.9%. The lowest flow rate did not alter Lyn-Src activity in MCF-10A mammary cells. This differential effect of varying flow rates on Lyn-Src has also been shown in chondrocytes under 3D interstitial fluid flow [48].

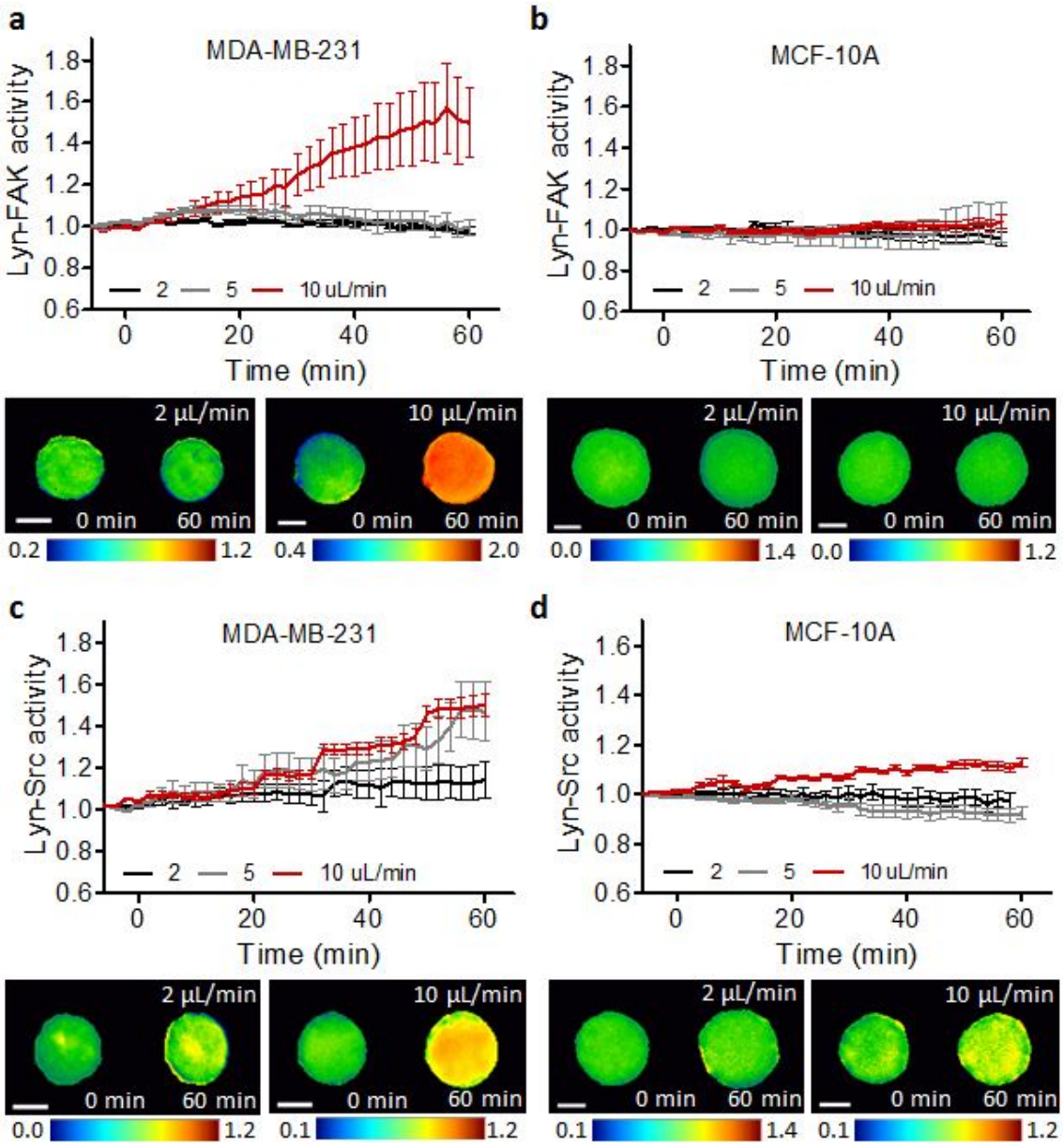

Fig. 3.1.: FAK and Src activities at the lipid raft of the plasma membrane. FRET ratio images were scaled according to the color bar, which represents the emission ratio CFP/YFP. (a) Lyn-FAK activity in MDA-MB-231 cells under fluid flow; n=10 (2 μL/min); n=8 (5 μL/min); n=8 (10 μL/min) cells. (b) Lyn-FAK activity in MCF-10A cells under interstitial fluid flow; n=10 (2 μL/min); n=11 (5 μL/min); n=11 (10 μL/min) cells. (c) Lyn-Src activity in MDA-MB-231 cells under IFF; n=9 (2 μL/min); n=9 (5 μL/min); n=8 (10 μL/min) cells. (d) Lyn-Src activity in MCF-10A cells under fluid flow; n=10 (2 μL/min); n=11 (5 μL/min); n=11 (10 μL/min) cells. Scale bar, 10 μm. * $p < 0.05$.

3.2 Interstitial fluid flow induces differential, subcellular AMPK activity in MDA-MB-231 cancer cells

AMPK is the cellular, metabolic stress regulator and a potential downstream target of Src and FAK, so subcellular AMPK activity was monitored in response to interstitial fluid flow. Metastatic breast cancer cells (MDA-MB-231) and non-tumor mammary cells (MCF-10A) were transfected with FRET-based biosensors specific to various subcellular domains of AMPK cytosol (Cyto-AMPK), mitochondria (Mito-AMPK), plasma membrane (PM-AMPK), and nucleus (Nuc-AMPK). Cells were then suspended in 3D in collagen-Matrigel, and the cell-gel mixture was inserted into flow chambers to polymerize. During imaging, samples were subjected to 2, 5, or 10 μL/min interstitial fluid flows [Fig. 3.2]. Subcellular AMPK activity was monitored via changes in the YFP/CFP emission ratio for each cell. Only MDA-MB-231 cells transfected with Mito-AMPK responded significantly to loading. The highest flow rate (10 μL/min) induced a 9.2% increase in Mito-AMPK activity after 60 minutes of interstitial fluid flow. Similarly, an intermediate flow rate of 5 μL/min prompted an 8.1% increase in activation. The lowest flow rate (2 μL/min) only increased the activity of Mito-AMPK by 3.7% at 60 minutes. This mild activation (less than 5% increase), while statistically significant, was not considered physiologically relevant. AMPK activity fluctuates in vivo; therefore, small changes in activity cannot be attributed to the effects of interstitial fluid flow. Unlike AMPK at mitochondria, Cyto-AMPK, PM-AMPK, and Nuc-AMPK were not activated by the applied levels of fluid shear stress in MDA-MB-231. Internal laboratory data also demonstrates differential, subcellular AMPK activation in 2D.

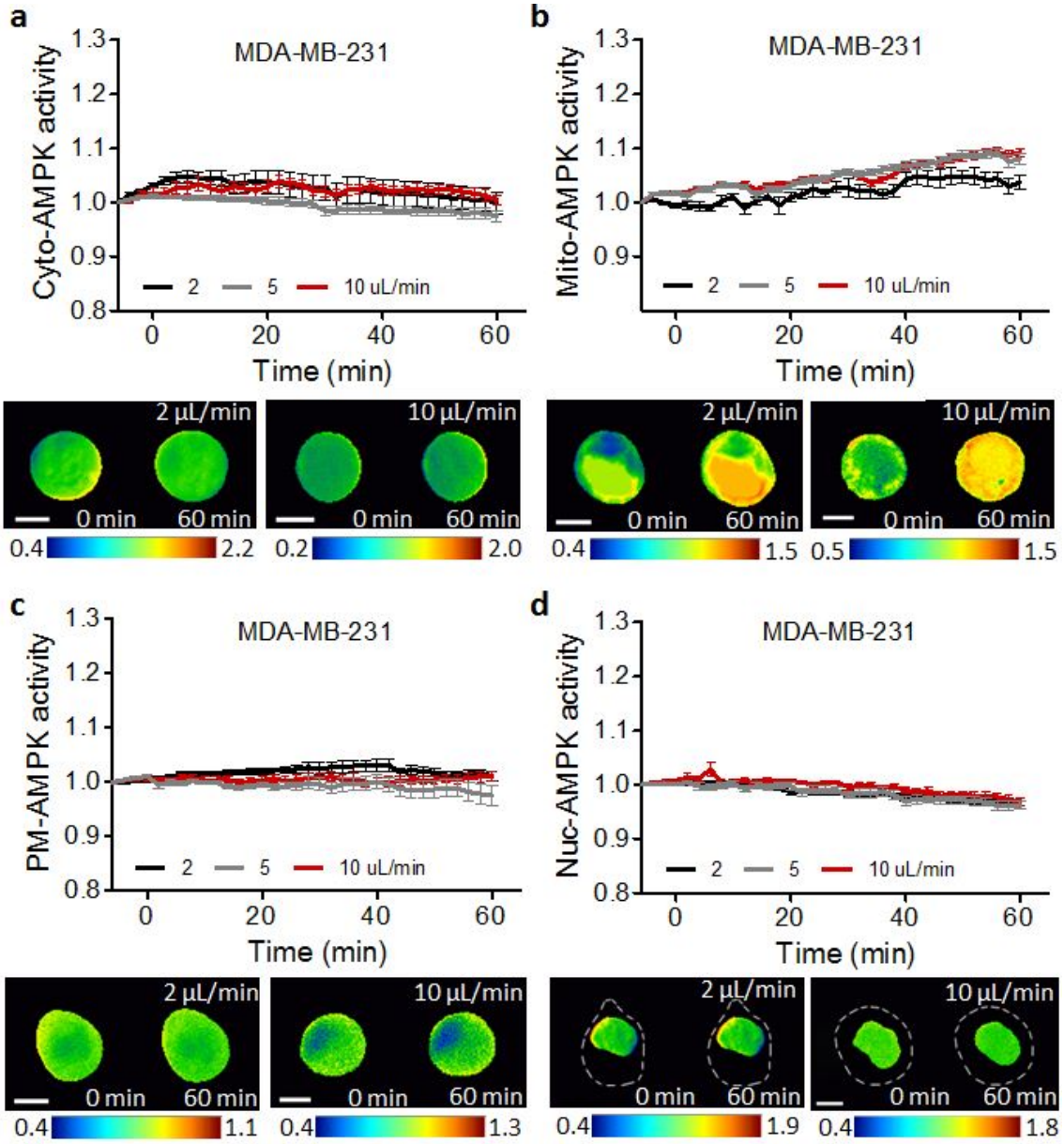

Fig. 3.2.: AMPK activities at subcellular domains of MDA-MB-231. FRET ratio images were scaled according to the color bar, which represents the emission ratio YFP/CFP. Interstitial fluid flow was applied at time = 0 min. (a) Cyto-AMPK activity under fluid flow; n=13 (2 μL/min); n=16 (5 μL/min); n=11 (10 μL/min) cells. (b) Mito-AMPK activity under interstitial fluid flow; n=12 (2 μL/min); n=14 (5 μL/min); n=13 (10 μL/min) cells. (c) PM-AMPK activity under fluid flow; n=11 (2 μL/min); n=11 (5 μL/min); n=12 (10 μL/min) cells. (d) Nuc-AMPK activity under fluid flow; n=14 (2 μL/min); n=12 (5 μL/min); n=16 (10 μL/min). Scale bar, 10 μm. * $p < 0.05$.

Unlike the breast cancer cell line (MDA-MB-231), subcellular AMPK in non-tumor mammary cells (MCF-10A) did not respond to interstitial fluid flow. AMPK activity was monitored in the cytoplasm, mitochondria, plasma membrane, and nucleus, but none of these organelles displayed domain-specific activation [Fig. 3.3].

It is worth noting that, similar to the 3D case, MDA-MB-231 metastatic cancer cells subjected to 2D fluid flow (a shear stress of 10 dyne/cm^2) displayed a 24.0% increase in Mito-AMPK activity. MCF-10A cells, however, did not alter their Mito-AMPK activity in response to the same high shear stress. Lower shear (2.5 dyne/cm^2) did not activate Mito-AMPK in either cell type in 2D. Therefore, fluid flow-induced activation of Mito-AMPK in MDA-MB-231 cells has been observed in both 2D and 3D. This information is important for the cohesiveness of migration experiments, where random migration assays were performed in 2D.

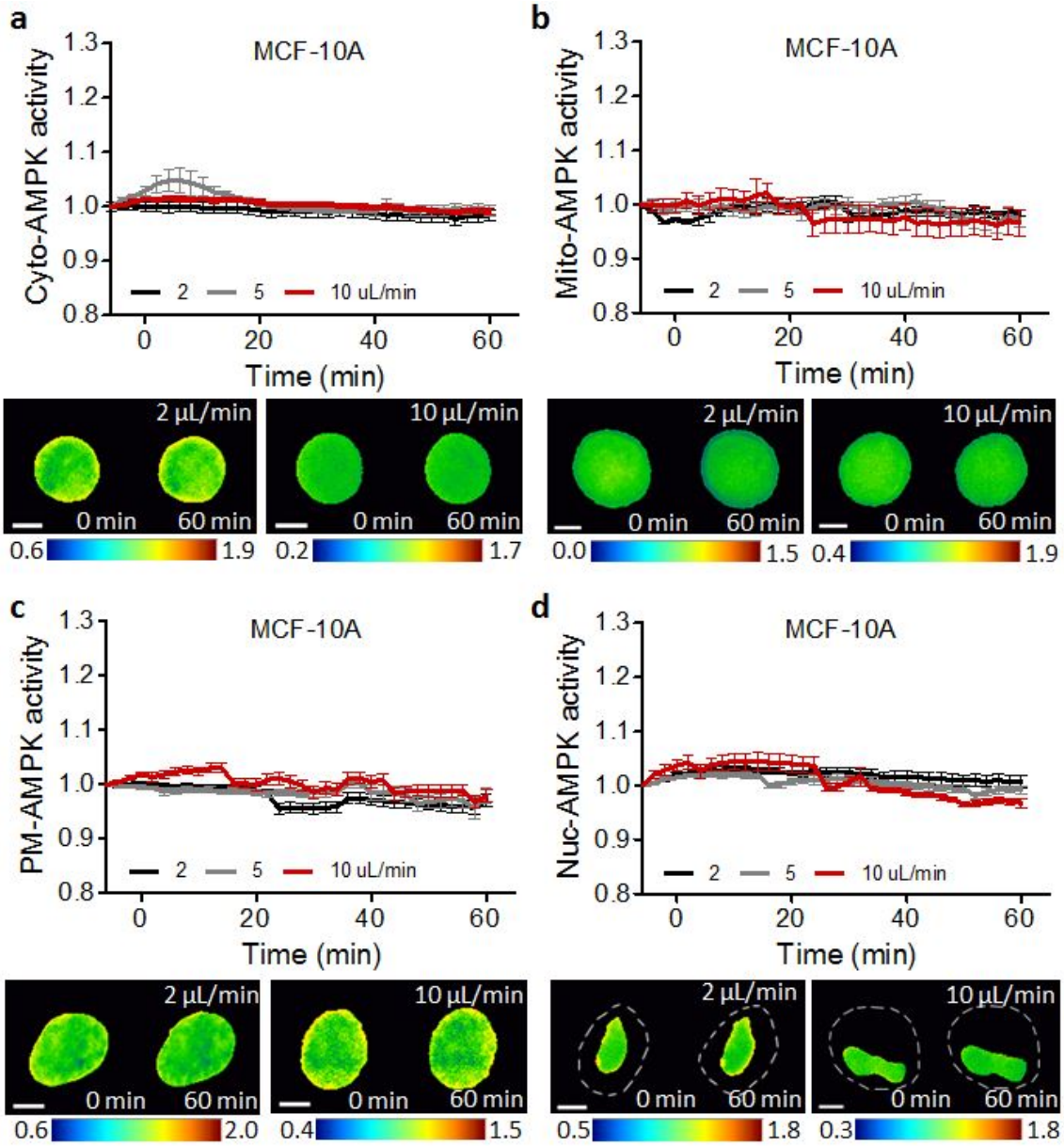

Fig. 3.3.: AMPK activities at subcellular domains of MCF-10A. FRET ratio images were scaled according to the color bar, which represents the emission ratio YFP/CFP. Interstitial fluid flow was applied at time = 0 min. (a) Cyto-AMPK activity under fluid flow; n=12 (2 μL/min); n=10 (5 μL/min); n=10 (10 μL/min). (b) Mito-AMPK activity under interstitial fluid flow; n=13 (2 μL/min); n=13 (5 μL/min); n=13 (10 μL/min). (c) PM-AMPK activity under fluid flow; n=14 (2 μL/min); n=14 (5 μL/min); n=14 (10 μL/min). (d) Nuc-AMPK activity under fluid flow; n=16 (2 μL/min); n=14 (5 μL/min); n=14 (10 μL/min). Scale bar, 10 μm. * $p < 0.05$.

3.3 Src or FAK inhibition abolishes Mito-AMPK activity and response to interstitial fluid flow in MDA-MB-231

To determine whether the activation of Mito-AMPK in MDA-MB-231 is downstream of FAK and Src, both FAK and Src were individually inhibited in 3D culture. MDA-MB-231 cells transfected with Mito-AMPK were embedded in collagen-Matrigel and placed in glass-bottom dishes. After a 2-hour incubation period, cells were treated with a Src inhibitor (PP2, 10 μM) or FAK inhibitor (PF573228, 1 μM). FRET images were acquired 1, 2, and 4 hours after drug treatment to monitor Mito-AMPK activity in comparison with an untreated control sample [Fig. 3.4]. Results showed a steady decline in the basal activity of Mito-AMPK over time. Both Src and FAK global inhibition resulted in consistently lower Mito-AMPK activity compared to the untreated cells. After 4 hours, cells treated with the FAK inhibitor (PF573228) showed a 9.2% decrease in Mito-AMPK activity, and cells treated with Src inhibitor (PP2) displayed a 10.3% decrease in Mito-AMPK activity.

Since Src and FAK inhibition significantly decreased Mito-AMPK activity in MDA-MB-231, we sought to determine whether similar inhibition could eliminate the shear stress-induced response of Mito-AMPK to interstitial fluid flow. MDA-MB-231 cells embedded in collagen gel were injected into flow chambers and incubated for 2 hours for gelation. Chambers were then treated with FAK inhibitor (PF573228, 1 μM) or Src inhibitor (PP2, 10 μM) and subjected to 10 μL/min fluid flow for 1 hour [Fig. 3.5]. While fluid flow alone increased Mito-AMPK activity by 9.2%, inhibition of either Src or FAK abolished this response. This showed that FAK and Src activation are required for the flow-mediated mechanotransduction of Mito-AMPK. The same is true for MDA-MB-231 cells cultured in 2D, according to internal laboratory data.

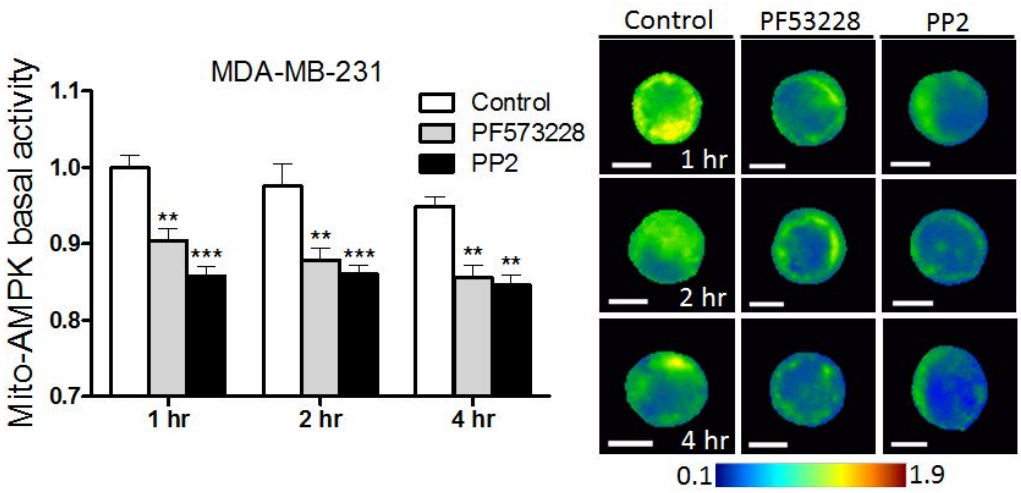

Fig. 3.4.: Mito-AMPK activity in MDA-MB-231 cells treated with kinase inhibitors for Src and FAK. After transfection, cells were treated with either 1 μM PP2 (Src inhibitor) or 10 μM PF573228 (FAK inhibitor). Mito-AMPK activity observed after 1, 2, and 4 hours of treatment. FRET ratio images scaled according to the color bar, which represents emission ratio YFP/CFP. Scale bar, 10μm. n>13 cells. * p<0.05.

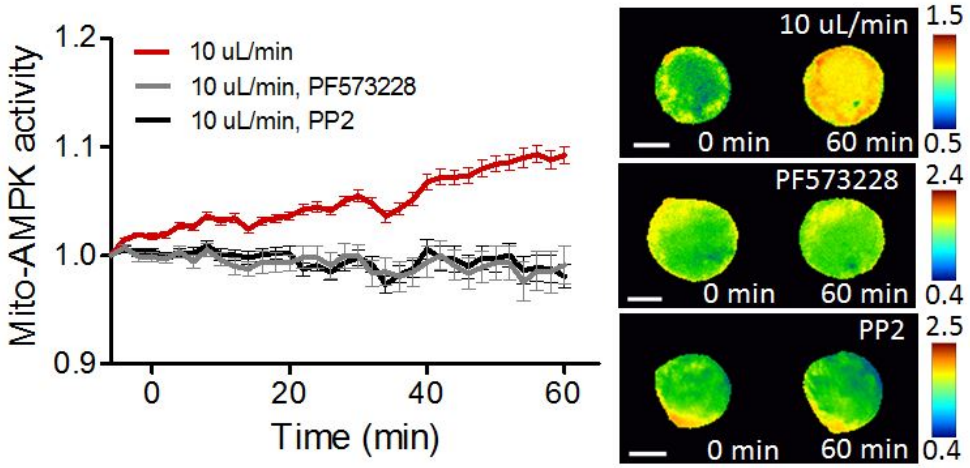

Fig. 3.5.: MDA-MB-231 cells transfected with Mito-AMPK were pretreated with either 1 μM PP2 (Src inhibitor) or 10 μM PF573228 (FAK inhibitor) for 1 hour before subjection to interstitial fluid flow (10 μL/min). Activation of Mito-AMPK by fluid flow was abolished by kinase inhibition. FRET ratio images scaled according to the color bar, which represents emission ratio YFP/CFP. Scale bar, 10μm. n>14 cells. * p<0.05.

3.4 Global AMPK activation reduces MDA-MB-231 cell migration

As mentioned previously, augmented global AMPK activity is known to attenuate cancer cell migration. To determine whether global AMPK activation reduces migration in MDA-MB-231 breast cancer cells, a random 2D migration assay was used. MDA-MB-231 cells were tagged with fluorescent GFP dye and seeded inside flow chambers at low confluency (10%). To study the general role of AMPK in cancer cell migration, some samples were treated with a global AMPK inhibitor (Compound C, 5 μM) or global AMPK activator (A769662, 25 μM). Individual cells, away from chamber walls and free to migrate, were tracked for 8 hours [Fig. 3.6.]. Results showed a significant decrease in cancer cell migration in response to global AMPK activation. The average cell displacement for untreated cells was 158.0 $\pm$ 6.8 μm, while the average displacement for cells treated with global AMPK activator (A769662) was only 104.0 $\pm$ 3.4 μm (a 34.2% decrease). Cells treated with AMPK global inhibitor (Compound C) displayed a slight increase in average cell migration (168.8 $\pm$ 5.4 μm), though it was not significant; however, this experiment does show that global AMPK activation affects cancer cell migration. These results are consistent with published reports on the linkage of global AMPK activation and the decreased migration or invasion of many cancers, including breast cancer [27, 28, 31].

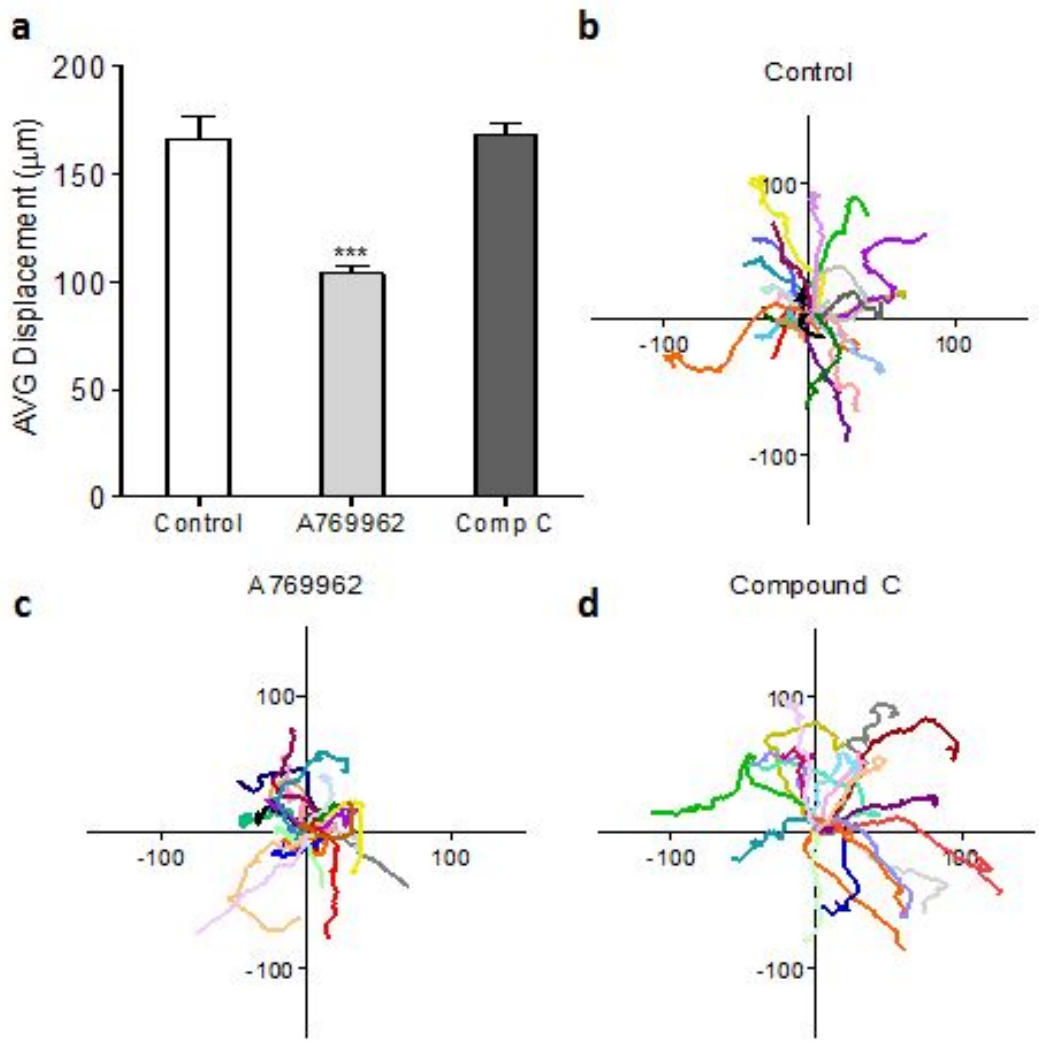

Fig. 3.6.: Random cell migration of MDA-MB-231 treated with global AMPK activator (A769962, 25 μM) or inhibitor (Compound C, 5 μM) 1 hour before imaging. (a) Bar graph showing the average displacement of cells over 8 hours; n=30 (control), n=54 (A769962), n=64 (Compound C) cells. * $p<0.05$. (b) Migration tracks (μm) for MDA-MB-231; n=25 cells. (c) Migration tracks (μm) for MDA-MB-231 treated with global AMPK activator; n=25 cells. (d). Migration tracks (μm) for MDA-MB-231 treated with global AMPK inhibitor; n=25 cells. The starting point for each cell migration track was normalized to the origin.

3.5 Mito-AMPK inhibition partially reduces cancer cell migration

While global AMPK activation has been shown to decrease cancer cell migration [27, 28, 31], some postulate that local AMPK activation at various subcellular

domains may play different or even antagonistic roles [29, 30, 33, 49]. As mentioned previously, cancer cells display decreased global AMPK activity [29, 30]. This leaves the metabolism of cancer cells unchecked, allowing them to grow, proliferate, and migrate more freely [15, 27, 28, 31]. It is also widely accepted that increased interstitial fluid flow at the tumor site induces metastasis [3–5, 7, 9]. However, as we have shown in this study, interstitial fluid flow increases subcellular Mito-AMPK activity in MDA-MB-231 cells. If fluid shear stress increases Mito-AMPK and migration simultaneously, then Mito-AMPK may have an augmenting, rather than inhibitory, effect on migration. To test this hypothesis, the role of Mito-AMPK in cancer cell migration was explored. MDA-MB-231 cells were transfected with a Mito-AMPK-specific inhibitory peptide (Tom20 AIP) and seeded in collagen-coated flow chambers. Individual cells were tracked for 8 hours in a random migration assay. Cells transfected with Tom20 AIP showed partially reduced migration [Fig. 3.7c]. The average cell displacement for Tom20 AIP transfected cells was 136.0 5.3 μm (13.9% decrease compared to control). To ensure that decreased migration was not simply a result of transfection, cells transfected with Mito-AMPK were also considered. Transfecting MDA-MB-231 with a FRET biosensor did not significantly affect migration [data not shown].

3.6 Mito-AMPK inhibition eliminates migration response to interstitial fluid flow

Next, we examined the effect of fluid flow on cancer cell migration, which is known to specifically increase Mito-AMPK activity. MDA-MB-231 cells were plated in collagen-coated flow chambers and subjected to 2D fluid flow. A peristaltic pump was used to apply shear flow at a volumetric flow rate of 10.6 mL/min, which corresponds to a 10 dyne/cm^2 shear stress. Cells subjected to 8 hours of unidirectional fluid flow showed a slight increase in cancer cell migration [Fig. 3.7d]. The average cell displacement was 171.7 $\pm$ 4.7 μm, which is an 8.0% increase compared to the control.

This affirmed the notion that fluid shear stress increases cancer cell metastatic potential. To determine whether Mito-AMPK activation in response to flow played a part in enhancing migration, cancer cells were both transfected with Tom20 AIP (Mito-AMPK inhibitor) and subjected to 10 dyne/cm^2 fluid flow [Fig. 3.7e]. Inhibition of Mito-AMPK completely abolished the migration response to fluid flow. The average cell displacement was reduced to 132.1 $\pm$ 6.9 μm (a 16.4% decrease). This suggests that Mito-AMPK activation was necessary for the flow-induced migration response of breast cancer cells. Since global AMPK activation is linked to suppressed cancer cell migration, yet flow-induced Mito-AMPK activation correlates with increased migration, one must assume that AMPK plays different roles in migration depending on its subcellular location.

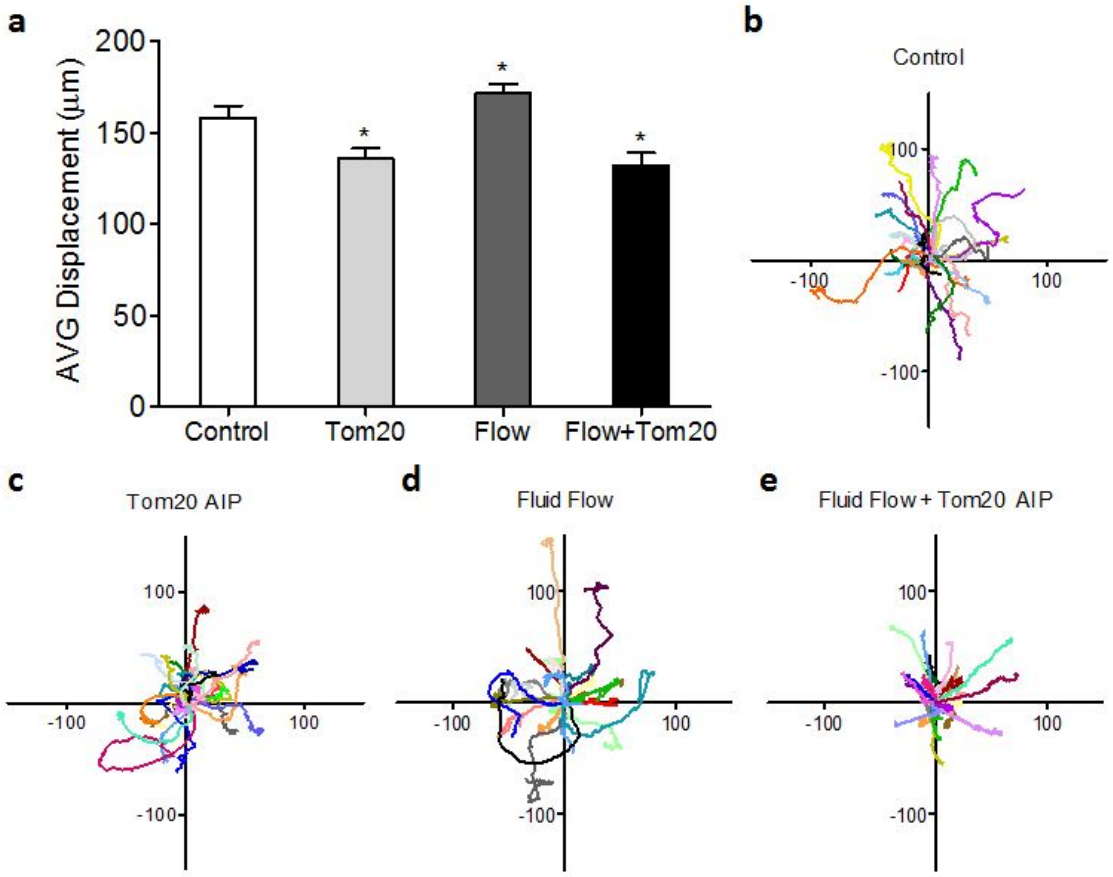

Fig. 3.7.: Random cell migration of MDA-MB-231 transfected with Mito-AMPK inhibitor peptide (Tom20 AIP), subjected to fluid flow (10 dyne/cm^2), or both. (a) Bar graph showing the average displacement of cells over 8 hours; n=30 (control), n=36 (Tom20 AIP), n=41 (fluid flow), n=39 (Tom20 AIP + fluid flow) cells. * $p<0.05$. (b) Migration tracks (μm) for MDA-MB-231; n=25 cells. (c) Migration tracks (μm) for MDA-MB-231 transfected with Mito-AMPK inhibitor (Tom20 AIP); n=25 cells. (d). Migration tracks (μm) for MDA-MB-231 subjected to fluid flow (10 dyne/cm2); n=25 cells. (e) Migration tracks (μm) for MDA-MB-231 transfected with Mito-AMPK inhibitor (Tom20 AIP) and subjected to fluid flow (10 dyne/cm^2); n=25 cells. The starting point for each cell migration track was normalized to the origin.

4. DISCUSSION

In this study we employed a 3D type I collagen-Matrigel model in conjunction with live cell imaging to determine the real-time activation of FAK, Src, and subcellular AMPK in response to interstitial fluid flow. Overall, MDA-MB-231 cancer cells were more mechanosensitive than MCF-10A non-tumor epithelial breast cells. Our results verified that mechanotransduction of membrane-bound FAK and Src is flow magnitude-dependent. For example, a low flow rate (2 μL/min) did not greatly activate Lyn-FAK or Lyn-Src in either MDA-MB-231 or MCF-10A cells. The highest flow rate (10 μL/min), however, increased Lyn-Src activity in both cell types and significantly increased Lyn-FAK activity in cancer cells. This data indicates a shear stress threshold for integrin-associated kinase activation in MCF-10A cells. A higher activation threshold in normal MCF-10A suggests that MDA-MB-231 cancer cells, which up-regulate Src and FAK expression, are more sensitive to mechanical stimulation [24–26].

We identified the metabolic regulator AMPK as a potential downstream target of FAK/Src signaling in response to fluid shear stress. In our study, interstitial fluid flow induced differential, subcellular AMPK activity in cancer cells. Since flow rates ranging from 2-10 μL/min are known to induce differential Src/FAK activation, subcellular AMPK activation along this integrin-mediated signaling axis must occur within the same range. Subcellular AMPK within MCF-10A normal epithelial cells did not respond to mechanical loading via IFF. In contrast, MDA-MB-231 metastatic cancer cells showed increased Mito-AMPK activation in a flow-magnitude dependent manner. Higher flow induced higher AMPK activity in the mitochondrial domain. To determine whether Mito-AMPK activity is Src/FAK-dependent, cancer cells were treated with Src or FAK inhibitors. Separate inhibition of Src or FAK reduced Mito-AMPK basal activity and abolished the response of Mito-AMPK to interstitial fluid

flow (10 μL/min). Whether the linkage between integrin/Src/FAK and Mito-AMPK is mechanical is unknown. Mitochondrial AMPK is located on the outer membrane of the organelles [28, 32, 50]. Activation of Mito-AMPK is required for mitochondrial turnover (mitophagy), fusion, and fission, enabling the dynamic plasticity of the mitochondria network in response to stress [28, 50]. Mitochondria localize preferentially along microtubules of the cytoskeleton, and they use microtubules as tracks to guide their movement within cells [33, 50–52]. It is possible that integrin-mediated signaling is transmitted via FAK/Src through the actin cytoskeleton, which connects to the microtubular network as well.

AMPK activation at mitochondria also plays a role in cell migration. Mitochondria regulate calcium homeostasis needed for polarity and cell migration [52]. MDA-MB-231 cancer cells cannot migrate effectively when mitochondrial genes for calcium regulatory proteins are perturbed [52]. During cell migration, mitochondria reposition strategically along microtubules, which polymerize toward cellular extensions [33, 51, 52]. Interestingly, AMPK controls the speed of microtubule polymerization toward focal adhesions [51]. Previous work showed localized, subcellular AMPK activation at mitochondria as they were trafficked toward the leading edge of cells during migration [33]. The results of our study also highlight the importance of Mito-AMPK activation in MDA-MB-231 cancer cell migration. Inhibition of Mito-AMPK partially reduces cell motility and abolishes the fluid flow-induced enhancement of migration. In contrast, global AMPK activation significantly reduced migration of MDA-MB-231. If global AMPK is down-regulated in cancer cells [27, 28, 31] and global AMPK activation reduces metastatic potential, how can subcellular AMPK activation at mitochondria promote migration? Our results affirm the notion that localized AMPK activities at various subcellular domains have dual (or even antagonistic) functions [28, 32, 33], particularly in MDA-MB-231 breast cancer migration. Our results suggest that the weighted net effect of these functions determines overall cell behavior.

5. CONCLUSIONS AND FUTURE DIRECTIONS

Breast tumors alter their biophysical environment by increasing ECM stiffness and interstitial fluid flow. High levels of IFF affect cancerous tissue differently than healthy mammary tissue, and shear stress stimulates integrin-mediated signaling within cancer cells. Ultimately, the mechanotransduction initiated at focal adhesions by IFF enhances cancer cell migration away from the primary tumor site as they invade the surrounding stroma. In this study, we have shown that integrin-associated kinases Src and FAK can be regulated by IFF. Similarly, subcellular AMPK can be differentially activated in MDA-MB-231 breast cancer cells by IFF along the Src-FAK signaling axis. We showed that global AMPK activation attenuates MDA-MB-231 breast cancer cell migration while fluid shear stress induces migration. Finally, it was revealed that subcellular AMPK activation at mitochondria is necessary for fluid flow-induced migration of MDA-MB-231 breast cancer cells. The dual, and somewhat contradictory, nature of AMPK at different domains suggests that fluid flow-induced migration of MDA-MB-231 is determined by the weighted net effect of subcellular AMPK activities. For conclusive results concerning breast cancer cell behavior, a more expansive variety of cell types should be used. Additionally, the domain-dependent signaling of AMPK is active in every metabolic process, not only migration. For future work, AMPK in other subcellular domains in cancer cell migration should be continued, and other behaviors, such as cell proliferation [15], should be explored.

LIST OF REFERENCES

LIST OF REFERENCES

[1] G. Dimri, H. Band, and V. Band, "Mammary epithelial cell transformation: insights from cell culture and mouse models," *Breast Cancer Research*, vol. 7, no. 4, p. 171, 2005.

[2] C.-H. Heldin, K. Rubin, K. Pietras, and A. Östman, "High interstitial fluid pressurean obstacle in cancer therapy," *Nature Reviews Cancer*, vol. 4, no. 10, p. 806, 2004.

[3] A. C. Shieh, "Biomechanical forces shape the tumor microenvironment," *Annals of biomedical engineering*, vol. 39, no. 5, pp. 1379–1389, 2011.

[4] M. J. Mitchell and M. R. King, "Computational and experimental models of cancer cell response to fluid shear stress," *Frontiers in oncology*, vol. 3, p. 44, 2013.

[5] W. J. Polacheck, J. L. Charest, and R. D. Kamm, "Interstitial flow influences direction of tumor cell migration through competing mechanisms," *Proceedings of the National Academy of Sciences*, vol. 108, no. 27, pp. 11 115–11 120, 2011.

[6] W. Yao, Y. Li, and G. Ding, "Interstitial fluid flow: the mechanical environment of cells and foundation of meridians," *Evidence-Based Complementary and Alternative Medicine*, vol. 2012, 2012.

[7] J. M. Munson and A. C. Shieh, "Interstitial fluid flow in cancer: implications for disease progression and treatment," *Cancer management and research*, vol. 6, p. 317, 2014.

[8] L. Chin, Y. Xia, D. E. Discher, and P. A. Janmey, "Mechanotransduction in cancer," *Current opinion in chemical engineering*, vol. 11, pp. 77–84, 2016.

[9] W. J. Polacheck, A. E. German, A. Mammoto, D. E. Ingber, and R. D. Kamm, "Mechanotransduction of fluid stresses governs 3d cell migration," *Proceedings of the National Academy of Sciences*, vol. 111, no. 7, pp. 2447–2452, 2014.

[10] D. Wirtz, K. Konstantopoulos, and P. C. Searson, "The physics of cancer: the role of physical interactions and mechanical forces in metastasis," *Nature Reviews Cancer*, vol. 11, no. 7, p. 512, 2011.

[11] R. Hansen and M. Bissell, "Tissue architecture and breast cancer: the role of extracellular matrix and steroid hormones." *Endocrine-Related Cancer*, vol. 7, no. 2, pp. 95–113, 2000.

[12] T. Oskarsson, "Extracellular matrix components in breast cancer progression and metastasis," *The Breast*, vol. 22, pp. S66–S72, 2013.

[13] M. A. Wozniak and P. J. Keely, "Use of three-dimensional collagen gels to study mechanotransduction in t47d breast epithelial cells," *Biological procedures online*, vol. 7, no. 1, p. 144, 2005.

[14] J. J. Yin, C. B. Pollock, and K. Kelly, "Mechanisms of cancer metastasis to the bone," *Cell research*, vol. 15, no. 1, p. 57, 2005.

[15] H. Motoshima, B. J. Goldstein, M. Igata, and E. Araki, "Ampk and cell proliferation–ampk as a therapeutic target for atherosclerosis and cancer," *The Journal of physiology*, vol. 574, no. 1, pp. 63–71, 2006.

[16] F. van Zijl, G. Krupitza, and W. Mikulits, "Initial steps of metastasis: cell invasion and endothelial transmigration," *Mutation Research/Reviews in Mutation Research*, vol. 728, no. 1, pp. 23–34, 2011.

[17] R. Kalluri and R. A. Weinberg, "The basics of epithelial-mesenchymal transition," *The Journal of clinical investigation*, vol. 120, no. 5, pp. 1786–1786, 2010.

[18] I. Beavon, "The e-cadherin–catenin complex in tumour metastasis: structure, function and regulation," *European journal of cancer*, vol. 36, no. 13, pp. 1607–1620, 2000.

[19] N. Pulo Jobe, D. Rosel, O. Tolde, J. Kosla, and J. Brábek, "Complex 3d models to study drug targeting of invadopodia," *Clinical Cancer Drugs*, vol. 1, no. 2, pp. 85–85, 2014.

[20] R. Singhai, V. W. Patil, S. R. Jaiswal, S. D. Patil, M. B. Tayade, and A. V. Patil, "E-cadherin as a diagnostic biomarker in breast cancer," *North American journal of medical sciences*, vol. 3, no. 5, p. 227, 2011.

[21] I. Y. Wong, S. Javaid, E. A. Wong, S. Perk, D. A. Haber, M. Toner, and D. Irimia, "Collective and individual migration following the epithelial–mesenchymal transition," *Nature materials*, vol. 13, no. 11, p. 1063, 2014.

[22] S. K. Mitra and D. D. Schlaepfer, "Integrin-regulated fak–src signaling in normal and cancer cells," *Current opinion in cell biology*, vol. 18, no. 5, pp. 516–523, 2006.

[23] A. Taherian, X. Li, Y. Liu, and T. A. Haas, "Differences in integrin expression and signaling within human breast cancer cells," *BMC cancer*, vol. 11, no. 1, p. 293, 2011.

[24] Y.-L. Tai, L.-C. Chen, and T.-L. Shen, "Emerging roles of focal adhesion kinase in cancer," *BioMed research international*, vol. 2015, 2015.

[25] C. M. Bagi, G. W. Roberts, and C. J. Andresen, "Dual focal adhesion kinase/pyk2 inhibitor has positive effects on bone tumors," *Cancer*, vol. 112, no. 10, pp. 2313–2321, 2008.

[26] R. Finn, "Targeting src in breast cancer," *Annals of Oncology*, vol. 19, no. 8, pp. 1379–1386, 2008.

[27] W. Li, S. M. Saud, M. R. Young, G. Chen, and B. Hua, "Targeting ampk for cancer prevention and treatment," *Oncotarget*, vol. 6, no. 10, p. 7365, 2015.

[28] A. S. Khan and D. E. Frigo, "A spatiotemporal hypothesis for the regulation, role, and targeting of ampk in prostate cancer," *Nature Reviews Urology*, vol. 14, no. 3, p. 164, 2017.

[29] G. Zadra, J. L. Batista, and M. Loda, "Dissecting the dual role of ampk in cancer: from experimental to human studies," *Molecular cancer research*, vol. 13, no. 7, pp. 1059–1072, 2015.

[30] B. Faubert, E. E. Vincent, M. C. Poffenberger, and R. G. Jones, "The amp-activated protein kinase (ampk) and cancer: many faces of a metabolic regulator," *Cancer letters*, vol. 356, no. 2, pp. 165–170, 2015.

[31] Y. Yan, O. Tsukamoto, A. Nakano, H. Kato, H. Kioka, N. Ito, S. Higo, S. Yamazaki, Y. Shintani, K. Matsuoka *et al.*, "Augmented ampk activity inhibits cell migration by phosphorylating the novel substrate pdlim5," *Nature communications*, vol. 6, p. 6137, 2015.

[32] T. Miyamoto, E. Rho, V. Sample, H. Akano, M. Magari, T. Ueno, K. Gorshkov, M. Chen, H. Tokumitsu, J. Zhang *et al.*, "Compartmentalized ampk signaling illuminated by genetically encoded molecular sensors and actuators," *Cell reports*, vol. 11, no. 4, pp. 657–670, 2015.

[33] B. Cunniff, A. J. McKenzie, N. H. Heintz, and A. K. Howe, "Ampk activity regulates trafficking of mitochondria to the leading edge during cell migration and matrix invasion," *Molecular biology of the cell*, vol. 27, no. 17, pp. 2662–2674, 2016.

[34] D. Kremers GJ, Piston DW. (1999) Basics of FRET microscopy nikon instruments inc. [Online]. Available: https://www.microscopyu.com/applications/fret/basics-of-fret-microscopy

[35] R. B. Sekar and A. Periasamy, "Fluorescence resonance energy transfer (fret) microscopy imaging of live cell protein localizations," *The Journal of cell biology*, vol. 160, no. 5, pp. 629–633, 2003.

[36] J. Seong, M. Ouyang, T. Kim, J. Sun, P.-C. Wen, S. Lu, Y. Zhuo, N. M. Llewellyn, D. D. Schlaepfer, J.-L. Guan *et al.*, "Detection of focal adhesion kinase activation at membrane microdomains by fluorescence resonance energy transfer," *Nature communications*, vol. 2, p. 406, 2011.

[37] Y. Wang, E. L. Botvinick, Y. Zhao, M. W. Berns, S. Usami, R. Y. Tsien, and S. Chien, "Visualizing the mechanical activation of src," *Nature*, vol. 434, no. 7036, p. 1040, 2005.

[38] J. Seong, S. Lu, M. Ouyang, H. Huang, J. Zhang, M. C. Frame, and Y. Wang, "Visualization of src activity at different compartments of the plasma membrane by fret imaging," *Chemistry & biology*, vol. 16, no. 1, pp. 48–57, 2009.

[39] M. Bizjak, P. Malavašič, K. Dolinar, J. Pohar, S. Pirkmajer, and M. Pavlin, "Combined treatment with metformin and 2-deoxy glucose induces detachment of viable mda-mb-231 breast cancer cells in vitro," *Scientific Reports*, vol. 7, no. 1, p. 1761, 2017.

[40] M. Rajh, K. Dolinar, K. Miš, M. Pavlin, and S. Pirkmajer, "Medium renewal blocks anti-proliferative effects of metformin in cultured mda-mb-231 breast cancer cells," *PloS one*, vol. 11, no. 5, p. e0154747, 2016.

[41] Ibidi. (2016) Shear stress and shear rates for ibidi -slides based on numerical calculations application note 11.

[42] G. M. Price and J. Tien, "Methods for forming human microvascular tubes in vitro and measuring their macromolecular permeability," in *Biological Microarrays*. Springer, 2011, pp. 281–293.

[43] S. Wang and J. M. Tarbell, "Effect of fluid flow on smooth muscle cells in a 3-dimensional collagen gel model," *Arteriosclerosis, thrombosis, and vascular biology*, vol. 20, no. 10, pp. 2220–2225, 2000.

[44] C. S. Hughes, L. M. Postovit, and G. A. Lajoie, "Matrigel: a complex protein mixture required for optimal growth of cell culture," *Proteomics*, vol. 10, no. 9, pp. 1886–1890, 2010.

[45] C. P. Ng and S. H. Pun, "A perfusable 3d cell–matrix tissue culture chamber for in situ evaluation of nanoparticle vehicle penetration and transport," *Biotechnology and bioengineering*, vol. 99, no. 6, pp. 1490–1501, 2008.

[46] B. D. Riehl, J. S. Lee, L. Ha, and J. Y. Lim, "Fluid-flow-induced mesenchymal stem cell migration: role of focal adhesion kinase and rhoa kinase sensors," *Journal of the Royal Society Interface*, vol. 12, no. 104, p. 20141351, 2015.

[47] J.-Y. Tinevez, N. Perry, J. Schindelin, G. M. Hoopes, G. D. Reynolds, E. Laplantine, S. Y. Bednarek, S. L. Shorte, and K. W. Eliceiri, "Trackmate: An open and extensible platform for single-particle tracking," *Methods*, vol. 115, pp. 80–90, 2017.

[48] Q. Wan, T. TruongVo, H. E. Steele, A. Ozcelikkale, B. Han, Y. Wang, J. Oh, H. Yokota, and S. Na, "Subcellular domain-dependent molecular hierarchy of sfk and fak in mechanotransduction and cytokine signaling," *Scientific reports*, vol. 7, no. 1, p. 9033, 2017.

[49] T. Isogai, J. S. Park, and G. Danuser, "Cell forces meet cell metabolism," *Nature cell biology*, vol. 19, no. 6, p. 591, 2017.

[50] C. J. L. T. L. O. H. K. Y. N. C. H. P. F. C. D. S. R. Toyama EQ, Herzig S, "Amp-activated protein kinase mediates mitochondrial fission in response to energy stress," *Science*, vol. 351, no. 6270, p. 275, 2016.

[51] A. Nakano, H. Kato, T. Watanabe, K.-D. Min, S. Yamazaki, Y. Asano, O. Seguchi, S. Higo, Y. Shintani, H. Asanuma *et al.*, "Ampk controls the speed of microtubule polymerization and directional cell migration through clip-170 phosphorylation," *Nature cell biology*, vol. 12, no. 6, p. 583, 2010.

[52] V. Paupe and J. Prudent, "New insights into the role of mitochondrial calcium homeostasis in cell migration," *Biochemical and biophysical research communications*, 2017.